Deep-Sea Research I 58 (2011) 241–259

Contents lists available at ScienceDirect

Deep-Sea Research I

journal homepage: www.elsevier.com/locate/dsri

Spatial variability and temporal dynamics of surface water pCO_2, $\Delta O_2/Ar$ and dimethylsulfide in the Ross Sea, Antarctica

P.D. Tortell [a,b,*], C. Guéguen [a,1], M.C. Long [c,2], C.D. Payne [a], P. Lee [d], G.R. DiTullio [d]

[a] Department of Earth and Ocean Sciences, University of British Columbia, 2146 Health Sciences Mall, Vancouver, BC, Canada V6T 1Z3
[b] Department of Botany, University of British Columbia, 6270 University Boulevard, Vancouver, BC, Canada V6T 1Z4
[c] Geological and Environmental Sciences, Stanford University, 473 Via Ortega, Stanford, CA 94305, USA
[d] Hollings Marine Laboratory, College of Charleston, 331 Fort Johnson, Charleston, SC 29412, USA

ARTICLE INFO

Article history:
Received 26 August 2010
Received in revised form
7 December 2010
Accepted 16 December 2010
Available online 4 January 2011

Keywords:
Ross Sea
CO_2
O_2/Ar
Dimethylsulfide
Mass spectrometry
Phaeocystis
Diatoms
Net community production
Air-sea exchange

ABSTRACT

We report results from two surveys of pCO_2, biological O_2 saturation ($\Delta O_2/Ar$) and dimethylsulfide (DMS) in surface waters of the Ross Sea polynya. Measurements were made during early spring (November 2006–December 2006) and mid-summer (December 2005–January 2006) using ship-board membrane inlet mass spectrometry (MIMS) for high spatial resolution (*i.e.* sub-km) analysis. During the early spring survey, the polynya was in the initial stages of development and exhibited a rapid increase in open water area and phytoplankton biomass over the course of our ~3 week occupation. We observed a rapid transition from a net heterotrophic ice-covered system (supersaturated pCO_2 and undersaturated O_2) to a high productivity regime associated with a *Phaeocystis*-dominated phytoplankton bloom. The timing of the early spring phytoplankton bloom was closely tied to increasing sea surface temperature across the polynya, as well as reduced wind speeds and ice cover, leading to enhanced vertical stratification. There was a strong correlation between pCO_2, $\Delta O_2/Ar$, DMS and chlorophyll *a* (Chl *a*) during the spring phytoplankton bloom, indicating a strong biological imprint on gas distributions. Box model calculations suggest that pCO_2 drawdown was largely attributable to net community production, while gas exchange and shoaling mixed layers also exerted a strong control on the re-equilibration of mixed layer O_2 with the overlying atmosphere. DMS concentrations were closely coupled to *Phaeocystis* biomass across the early spring polynya, with maximum concentrations exceeding 100 nM.

During the summer cruise, we sampled a large net autotrophic polynya, shortly after the seasonal peak in phytoplankton productivity. Both diatoms and *Phaeocystis* were abundant in the phytoplankton assemblages during this time. Minimum pCO_2 was less than 100 ppm, while $\Delta O_2/Ar$ exceeded 30% in some regions. Mean DMS concentrations were ~2-fold lower than during the spring, although the range of concentrations was similar between the two surveys. There was a significant correlation between pCO_2, $\Delta O_2/Ar$ and Chl *a* across the summer polynya, but the strength of these correlations and the slope of O_2 vs. CO_2 relationship were significantly lower than during the early spring. Summertime DMS concentrations were not significantly correlated to phytoplankton biomass (Chl *a*), pCO_2 or $\Delta O_2/Ar$. In contrast to the early spring time, there were no clear temporal trends in summertime gas concentrations. Rather, small-scale spatial variability, likely resulting from mixing and localized sea-ice melt, was clearly evident in surface gas distributions across the polynya. Analysis of length-scale dependent variability demonstrated that much of the spatial variance in surface water gases occurred at scales of <20 km, suggesting that high resolution analysis is needed to fully capture biogeochemical heterogeneity in this system.

1. Introduction

The Ross Sea polynya is one of the most biologically productive regions in the Southern Ocean (Smith and Gordon, 1997; Arrigo et al., 1998b) and an important site of deep water formation (Jacobs, 2004; Trumbore et al., 1991). By virtue of its high primary productivity and seasonal ice cover, this region constitutes a

* Corresponding author at: Department of Earth and Ocean Sciences, University of British Columbia, 2146 Health Sciences Mall, Vancouver, BC, Canada V6T 1Z3. Tel.: +1 604 822 4728; fax: +1 604 822 6091.
E-mail address: ptortell@eos.ubc.ca (P.D. Tortell).
[1] Current address: Department of Chemistry, Trent University, 1600 West Bank Drive, Peterborough, ON, Canada K9J 7B8.
[2] Current address: National Center for Atmospheric Research, 1850 Table Mesa Drive, Boulder, CO 80305, USA.

0967-0637/$ - see front matter © 2011 Elsevier Ltd. All rights reserved.
doi:10.1016/j.dsr.2010.12.006

strong sink for atmospheric CO_2, with a significant capacity for carbon transport into the ocean interior (Sandrini et al., 2007; Arrigo et al., 2008). Large fluxes of the climate-active gas dimethylsulfide (DMS) have also been documented in the Ross Sea polynya (Ditullio and Smith, 1995; Kiene et al., 2007). DMS concentrations in this region are among the highest in the world's oceans (Kettle et al., 1999), and the resulting sea-air DMS fluxes constitute a significant source of sulfur aerosols to the atmosphere (Gondwe et al., 2003). These aerosols backscatter incoming solar radiation and act as cloud condensation nuclei, influencing the atmospheric albedo (Boucher et al., 2003). The factors governing the distribution of DMS and pCO_2 in the Ross Sea are therefore of significant biogeochemical and climate relevance, and have been the focus of intensive field measurement programs (Smith et al., 2000; DiTullio and Dunbar, 2003).

In the Ross Sea, as in all marine systems, variability in surface water gas is generated by the interplay of ocean mixing, air-sea exchange and biological cycling. Net community production (NCP; *i.e.* photosynthesis minus respiration) consumes CO_2 and releases O_2, effectively coupling these two gases in the mixed layer. The magnitude of NCP depends upon surface ocean nutrient supply and mean irradiance levels, both of which are strongly influenced by vertical stratification and mixed layer depths (MLD). Surface DMS concentrations are also influenced by mixed layer dynamics, phytoplankton species composition and productivity, and photochemical processes (see reviews by Simó (2004) and Stefels et al. (2007). This volatile compound is derived from the algal metabolite dimethylsulfoniopropionate (DMSP), which is released into the water column through various trophic processes including algal excretion, zooplankton grazing and viral lysis (Dacey and Wakeham, 1986; Belviso et al., 1990; Malin et al., 1998), and subsequently cycled through the microbial loop (Kiene and Linn, 2000; Zubkov et al., 2002). Empirical algorithms have been developed to predict global DMS distributions based on surface ocean Chl *a* concentrations, mixed layer depths and solar radiation dose (Simo and Dachs, 2002; Vallina et al., 2007). These algorithms perform relatively well over large spatial scales, but they cannot resolve mesoscale and sub-mesoscale DMS variability (Derevianko et al., 2009), which is apparent in many oceanic regions (*e.g.* Kiene et al., 2007; Nemcek et al., 2008). This small-scale variability results, in large part, from the rapid turnover of DMS in the mixed layer, associated with high rates of biological consumption and photo-oxidation (Simó et al., 2000; Toole et al., 2004; Merzouk et al., 2006; del Valle et al., 2009).

Biogeochemical processes in the Ross Sea vary dramatically over the course of the seasonal cycle in response to changing solar irradiance, wind speeds and ice cover (Arrigo et al., 1998a). During winter, cooling and brine rejection drive deep convection, resulting in a vertically homogenous, net heterotrophic water column that is supersaturated in pCO_2 and undersaturated in O_2 (Sweeney et al., 2000). During this time, significant ice cover acts to restrict air-sea exchange and thus limits the equilibration of surface waters with the overlying atmosphere. As ice clears in spring and surface waters warm, stratification and an increasing photoperiod promote high rates of primary productivity causing rapid pCO_2 drawdown, and O_2 and DMS accumulation. As the growing season progresses, differences in winds and sea-ice melt contributions drive regional variability in sea ice cover and stratification. For example, very shallow (*i.e.* < 15 m) mixed layers are produced by ice melt in the NW polynya (*e.g.* Terra Nova Bay) during summertime conditions (Arrigo et al., 1998a). This region can exhibit extreme pCO_2 drawdown (*i.e.* $pCO_2 < 100$ ppm; Sweeney et al., 2000) and typically supports phytoplankton communities dominated by diatoms rather than *Phaeocystis antarctica*, a colonial haptophyte that is dominant elsewhere in the Ross Sea polynya (DiTullio and Smith, 1996; Arrigo et al., 2000; Sweeney et al., 2000). These two taxa have different C:N:P uptake stoichiometries, rates of export production and DMS(P) production (Arrigo et al., 2002). Stratification-induced patterns coupled with iron limitation effects on diatom and *Phaeocystis* abundances (Sedwick et al., 2000) can thus drive spatial variability in surface water biogeochemical cycles (Arrigo et al., 1999, 2002).

In addition to large-scale gradients due to ice melt, stirring and lateral advection can result in variability in mixing depths and gas distributions over a range of scales. These processes have gained recognition recently as important controls on mixed layer depth (Boccaletti et al., 2007; Fox-Kemper et al., 2008; Thomas and Ferrari, 2008) and primary productivity (Long et al., submitted for publication-a), thus driving small-scale heterogeneity in surface gas concentrations. Since biogeochemical and physical processes are inherently non-linear, resolving this small-scale variability is important to develop an accurate description picture of surface ocean gas distributions and sea-air fluxes.

Biogeochemical sampling at discrete hydrographic stations cannot adequately resolve sub-mesoscale variability in the Ross Sea and other dynamic marine systems (Hales and Takahashi, 2004). To address this limitation, we and others have developed a new approach to underway ship-board gas measurements using membrane inlet mass spectrometry (MIMS, Kaiser et al., 2005; Tortell, 2005). With this method, it is possible to simultaneously examine variability in pCO_2, DMS and O_2/Ar at sub-km spatial scales (Tortell and Long, 2009). The O_2/Ar ratio provides information on biological O_2 cycling, since Ar normalization corrects for physically induced changes in O_2 saturation state such as temperature changes and bubble injection (Craig and Hayward, 1987). Coupled measurements of O_2/Ar and pCO_2 thus provide significant insight into surface water NCP and biological C cycling in oceanic surface waters.

In this paper, we report the results of a two-year field survey of dissolved gas concentrations in the Ross Sea polynya, using ship-board MIMS for high resolution measurements of surface water pCO_2, DMS and O_2/Ar. We conducted cruises during the austral spring bloom and early summer phytoplankton growth seasons under different physical, chemical and biological conditions, and we compare and contrast the two field seasons in terms of gas concentrations and hydrographic/biological variability. Our primary objective was to characterize the temporal and spatial heterogeneity of surface water gases in the Ross Sea to gain insight into seasonal biogeochemical dynamics and the relevant scales of underlying variability.

2. Methods

Two underway surveys of the Ross Sea polynya were conducted on board the R.V./IB *Nathaniel B. Palmer* as part of the CORSACS program (Control on Ross Sea Algal Community Structure). The surveys were conducted during the early phytoplankton growing season (November 11, 2006–December 4, 2006: CORSACS II), when phytoplankton assemblages were dominated by *P. antarctica*, and the later growth season (December 26, 2005–January 24, 2006: CORSACS I) when blooms of both *Phaeocystis* and diatoms were present. We note that the two cruises did not occur contiguously over the same growing season; as a result interannual variability could affect the interpretation of our results. Below, we refer to CORSACS II (C2) as the early phytoplankton growing season and CORSACS I (C1) as the mid-season period, following the bloom peak.

2.1. Continuous underway sampling system

Simultaneous underway measurements of pCO_2, O_2/Ar ratios and DMS were conducted using membrane inlet mass spectrometry

(MIMS) (Tortell, 2005). Seawater samples were obtained from the ship's uncontaminated underway system, located at the bow at a nominal depth of ~5 m. In order to reduce membrane permeability changes due to temperature variability, water samples were introduced into the cuvette at constant temperature (2.5 °C). Temperature equilibration of samples was achieved using a heat exchanger (20 ft of 1/4 in stainless steel tubing) immersed in a temperature-controlled water bath (VWR Scientific, USA). Data were collected more than twice per minute, yielding an effective spatial resolution of ~100–200 m along the cruise track (with closer spacing during transits through sea-ice or when towing underway sampling equipment). Instrument response time, including membrane permeation and ion detection, was less than 20 s for gases.

2.2. Calibration of dissolved gases

The instrument ion current intensities obtained at *m/z* (mass to charge ratio) 32, 40, 44 and 62 were calibrated using equilibrated seawater standards for CO_2 and O_2/Ar, and DMS seawater standards. CO_2 and DMS calibrations were performed once per day, while ΔO_2/Ar calibrations were performed several times per day. This frequency was sufficient to constrain instrument drift. The flow rate (~300 mL min^{-1}) and sample temperature (2.5 °C) during calibration were the same as during the underway data acquisition, and approximately 500 mL of each standard was used to calibrate the MIMS. DMS calibration was performed as described by Nemcek et al. (2008).

For CO_2, the primary standards consisted of 4 L polycarbonate bottles with prefiltered seawater (<0.2 μm, Whatman Polycap Capsule) gently bubbled through a diffusing stone with dry CO_2 gas mixtures (100, 380 and 800 ppm, balance air; Scott Specialty Gases, CA). Prefilters were rinsed with 10% HCl and stored at 4 °C in between uses. For C1, these CO_2 seawater standards were kept in a flow-through deck-board incubator at *in-situ* sea surface temperature (SST) for at least 2 days prior to use. Discrete subsamples (500 mL) were drawn into glass bottles from each primary standard for measurement on the MIMS. The reproducibility of the standard measurements was better than 0.3% over 5 days (see Gueguen and Tortell (2008) for further details). For C2, CO_2 standards were kept in a laboratory temperature equilibration tank connected to the ship's flowing surface seawater supply. Subsamples were removed directly from bottles via electronic switching valves (Valco Instruments) connected to the seawater sampling system. After three point calibration using the equilibrated seawater standards, pCO_2 measurements were calculated at *in-situ* temperature using empirical equations (Takahashi et al., 2009). The continuous pCO_2 values obtained by MIMS were in good agreement with those obtained by the underway pCO_2 LI-COR analyzer deployed on the R.V./IB *Nathaniel B. Palmer*, with a mean offset of 1.4 and 4.9 μatm for C1 and C2, respectively.

For O_2/Ar ratios, air-equilibrated standards consisted of 4 L polycarbonate bottles with prefiltered seawater (<0.2 μm, Whatman Polycap Capsule) gently bubbled with ambient laboratory air through a diffusing stone. For C1, standard bottles were maintained in a temperature-controlled chamber at 0 (±1)°C and 100% humidity for at least 24 h prior to calibrations. For C2, temperature control was achieved using the laboratory temperature equilibrator tank described above for CO_2 standards. O_2/Ar measurements (the ratio of ion currents at *m/z* 32 and 40) were expressed as a percent saturation anomaly (ΔO_2/Ar) (Emerson et al., 1999) relative to the O_2/Ar ratio measured in air-equilibrated seawater samples several times per day

$$\Delta O_2/Ar = [(O_2/Ar)_{meas.}/(O_2/Ar)_{sat.} - 1] * 100 \quad (1)$$

For C2, we collected a number of discrete calibration samples for surface water O_2/Ar ratios. These samples were collected from 5 m Niskin bottle casts using the procedure and equipment described by Emerson et al. (1999). Samples were analyzed in the laboratory via isotope ratio mass spectrometry (IRMS) several months after collection as previously described (Emerson et al., 1999). Comparison of our underway ΔO_2/Ar measurements with the discrete IRMS calibration samples showed very good agreement between MIMS and IRMS data (*see* Fig. 7), with a mean deviation of −0.18% ($n=10$) between the two methods.

2.3. C–O stoichiometry

To examine the stoichiometric relationship between C and O in the mixed layer we converted our ΔO_2/Ar and pCO_2 data to O_2 and dissolved inorganic carbon (DIC) concentrations. We used the strong linear relationship between ΔO_2/Ar and O_2 concentrations derived from >150 surface bottle casts over both C1 and C2 ($r^2=0.95$) to calculate O_2 concentrations from our high resolution surface measurements. Similarly, we used a logarithmic fit ($r^2=0.96$) to surface bottle observations for C1 and C2 to convert pCO_2 into salinity-normalized DIC.

2.4. Sea-air gas fluxes

We used our surface concentration measurements and ship-based wind-speed data to calculate sea-air fluxes for O_2, CO_2 and DMS. We computed sea-air exchange of CO_2 as

$$F_{CO_2} = (1-A)k_{CO_2}\gamma(pCO_2^{sw} - pCO_2^{atm}) \quad (2)$$

where A is the fraction of sea surface covered by ice, γ is the SST- and salinity-dependent solubility of CO_2 (Weiss, 1974), and k_{CO_2} is the gas transfer velocity (cm h^{-1}), calculated as a function of wind speed and the temperature-dependent Schmidt number (Wanninkhof, 1992). We assume a constant value for pCO_2^{atm} of 375 μatm. O_2 fluxes were computed as

$$F_{O_2} = (1-A)k_{O_2}(\Delta O_2/Ar)O_{2_{sat}}$$

where k_{O_2} is the piston velocity for sea-air O_2 exchange and $O_{2_{sat}}$ is the temperature and salinity dependent equilibrium O_2 concentration, calculated using the equations of Garcia and Gordon (1992). For DMS, since atmospheric concentrations are often assumed to be negligible, we compute sea-air flux as

$$F_{DMS} = (1-A)k_{DMS}(DMS_{sw}) \quad (3)$$

where DMS_{sw} is the concentration of DMS in the surface ocean and k_{DMS} is the piston velocity of Wanninkhof (1992), normalized to the Schmidt number for DMS of Saltzman et al. (1993). Recent work has suggested that the Wanninkhof (1992) formulation may overestimate the piston velocity for DMS at wind speeds above 10 m s^{-1} (Vlahos and Monahan, 2009), and our sea-air fluxes may thus represent upper bounds in regions of high wind speed. Similarly, our flux calculations may be overestimates if atmospheric DMS concentrations are non-negligible as we have assumed. Non-negligible DMS concentrations could result from a combination of high sea-air fluxes and a small atmospheric sink term. Unfortunately, there are no direct atmospheric DMS measurements from our cruise.

We computed the sea-air flux of CO_2, O_2 and DMS for each gas concentration measurement along the cruise track. We forced the computation with 24-h running-mean wind speed from the ship's anemometer and SSM/I ice concentration data (25 km resolution) (Cavalieri et al., 1990) interpolated to the cruise track. We calculated solubility and Schmidt numbers using ship-based SST and salinity observations. To estimate a representative value of sea-air exchange rates, we aggregated these flux estimates, made approximately every ~1 min, into daily means.

2.5. Surface DMS by gas chromatography

During C1 and C2, discrete samples from Niskin bottles on the CTD-Rosette were collected using standard sampling procedures for the measurement of dissolved gases. During C2, additional discrete samples were also collected using the same sampling protocol from the ship's continuous supply while the ship was on-station for CTD-Rosette sampling. Samples from either the Niskin bottles or continuous supply were transferred to BOD bottles using silicone tubing and filled carefully to avoid trapping bubbles in sample bottles. Samples for the analysis of DMS were then collected following the small-volume, gravity-filtration methodology of Kiene and Slezak (2006). A small aliquot of each sample ($\leq$15 mL) was gravity-filtered through a 25 mm Whatman GF/F filter and the filtrate collected for the immediate determination of DMS. All sample processing was carried out in a cold room at $\sim$0 °C. DMS was measured using a cryogenic purge and trap system coupled to a Hewlett-Packard 5890 Series II gas chromatograph fitted with a Chromosil 330 packed column (Supelco Inc.) and flame photometric detector (DiTullio and Smith, 1995b). The instrument was calibrated using both constant-temperature DMS permeation devices (Vici Metronics) and DMSP standards (Research Plus Inc.), with base hydrolysis using 2 mol L^{-1} sodium hydroxide. The detection limit was 0.2 nM for 50 mL samples, and the relative standard deviation was better than 9% for triplicate standards.

2.6. Phytoplankton biomass and hydrographic data

Measurements of SST ($\sim$5 m) and salinity were logged continuously from the ship's thermosalinograph (SeaBird Model SBE-21) while continuous sea surface Chl *a* fluorescence (used as a proxy for bulk phytoplankton biomass) was recorded by ship's underway sensor (Turner, 10-AU-005). These variables were averaged into one minute sampling bins and aligned with underway gas data.

Total phytoplankton biomass and taxonomic composition were also assessed using HPLC analysis of Chl *a* and accessory photosynthetic pigment concentrations. Seawater for pigment analysis was obtained from the underway seawater system every $\sim$20 km along the ship's track. Samples were collected on glass fiber filters (GF/F, nominal pore size 0.7 μm), frozen in liquid N_2 and returned to the laboratory for subsequent analysis. In the laboratory, pigments were extracted in 90% acetone for at least 24 h at 4 °C and quantified using the method described elsewhere (DiTullio and Geesey, 2002). We used diagnostic marker pigments for different phytoplankton groups (*e.g.* 19-Hex and $Chlc_3$ for *Phaeocystis*) to assess the taxonomic composition of phytoplankton assemblages, employing the CHEMTAX algorithm as described by Mackey et al. (1996).

2.7. Statistical analysis

Pair-wise Pearson correlation coefficients were computed to examine the relationships between gases and other hydrographic measurements along the ship's track. To quantify the length scales of spatial variability for gases and hydrographic parameters along our cruise tracks, we used the approach of Hales and Takahashi (2004), using a structure function to estimate interpolation errors associated with low resolution data sampling. For this analysis, we selected a number of linear sections along our cruise track that were $>$200 km long and contained no data gaps. For each of these track sections, data were sub-sampled at increasing distance intervals, and the lower resolution data sets were linearly interpolated to the spatial resolution of the original measurements ($\sim$0.2 km). The difference between actual measurements and interpolated values was used to derive a root mean square error as a function of sampling distance. The interpolation errors increase as sampling distance increases until a plateau is reached, corresponding to the total variance of the dataset. The increase in sampling error with increasing distance is well described by a first-order exponential rise function:

$$E_x = E_\infty(1-\exp(-x/x_{char})) \quad (4)$$

where E_x is the sampling error at distance x, E_∞ is the asymptotically approached maximum sampling error and x_{char} is a characteristic length scale at which $\sim$63% of E_∞ is attained (see Hales and Takahashi (2004) for further details and examples). We used a Levenberg–Marquardt non-linear regression algorithm (SigmaPlot) to fit this equation to our interpolation error curves and obtain least-squares parameter values for E_∞ and x_{char}.

2.8. Box model simulations

We used a simple 1-D box model to examine the relative influence of sea-ice modulated gas exchange, NCP, and MLD on the evolution of surface pCO_2 and $\Delta O_2/Ar$ during the Ross Sea spring bloom. The model is not intended to represent the time-dependent evolution of mixed layer pCO_2 and $\Delta O_2/Ar$ with full accuracy. Rather, it provides an internally consistent framework to examine how gas concentrations scale with respect to different physical and biological forcing. The model results are thus idealized solutions, intended to provide reference for the observations, and examine the time-dependent evolution of surface gas concentrations in reference to mixed layer depth, gas exchange and NCP. Comparing our observations with the calculated model responses associated with a range of forcing permits inferences regarding the likely influence of these variables on mixed layer pCO_2 and $\Delta O_2/Ar$.

The model, described in detail by Long (2010), is similar in structure to that presented by Gruber et al. (1998). The time-integrated mass balance of carbon and oxygen in the mixed layer is defined by

$$\frac{\partial C}{\partial t} = J_{diff} + J_{ent} + J_{ex} + J_{ncp}$$

where the four right hand terms represent; fluxes due to turbulent diffusion at the base of the mixed layer, entrainment associated with changes in mixed layer depth, air-sea gas exchange and net community production. In our simulations, we neglected the turbulent diffusive flux term. This process acts to drive mixed layer tracer concentrations back towards deep water (*i.e.* wintertime) values, and thus diminish the rate of change observed in surface waters. Although turbulent diffusion across the base of the mixed layer is likely significant in a poorly stratified system such as the Ross Sea, the magnitude of this process is poorly constrained. We also neglect vertical entrainment fluxes associated with mixed layer deepening, a process which has the same effect on surface water tracers as vertical diffusivity across the base of the mixed layer. We neglect this entrainment flux since mixed layer depths showed a strong shoaling trend during the early spring cruise, associated with significant surface warming and decreased wind speeds. The simplifying assumptions we used in our box model calculations do not affect the conclusions we draw on the relative influence of gas exchange, mixed layer depth and NCP on surface water O_2 and C budgets.

We used ship-based daily mean wind speeds and sea ice concentrations from SSM/I (Cavalieri et al., 1990) interpolated to cruise track to force the model, and ran calculations with a daily time-step, spanning a range of NCP values and mixing depths.

We used constant mixing depths and NCP for each individual simulation, and performed repeated calculations using a range of values for these variables. Calculations were performed separately for the first 9 days of our survey prior to the onset of the large phytoplankton bloom, and the last 10 days when phytoplankton biomass increased rapidly (though non-monotonically) across the polynya.

3. Results

3.1. Sea ice and hydrographic conditions

Our two surveys were conducted under contrasting hydrographic and sea ice conditions in the Ross Sea polynya. During the austral spring bloom (C2), the polynya was in the initial stages of development, with significant ice cover (40–70%) across much of the sampling region (Fig. 1a). During the ~3 weeks of our survey, the area of ice-free waters increased ~3-fold, from 0.4 to 1.75 10^5 km^2 (Long et al., submitted for publication-b). During the summer season (C1 survey), much of the Ross Sea polynya was ice free, with significant ice cover (> 50%) only observed along the Ross Ice Shelf and in the Western region along Terra Nova Bay (Fig. 1b).

Polynya surface waters were relatively homogeneous with respect to SST and salinity (Figs. 2 and 3) during C2 cruise; SSTs were generally within 1 °C of the freezing point across our survey region (mean -1.7 ± 0.2 °C), while salinity generally exceeded

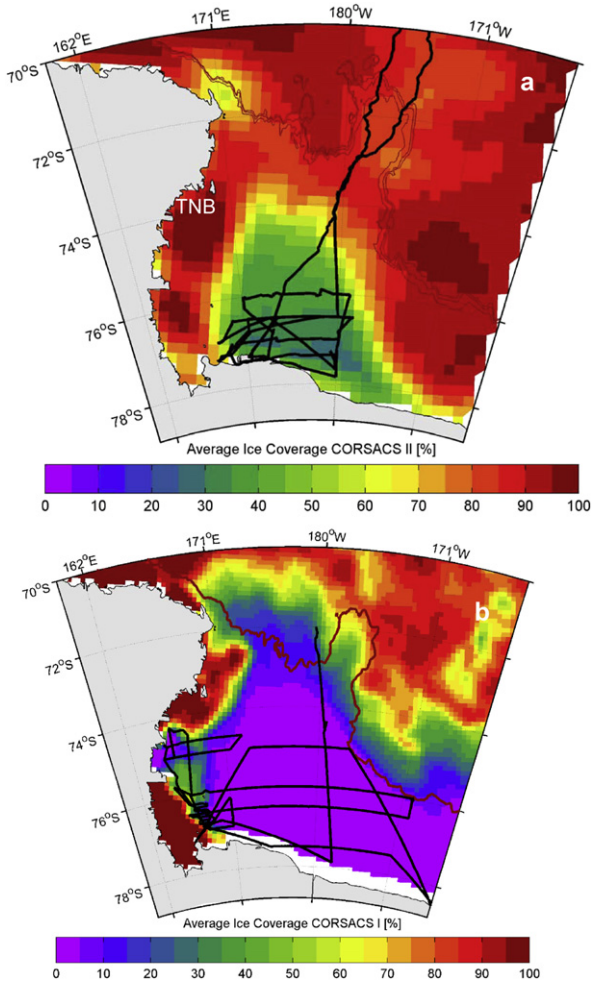

Fig. 1.

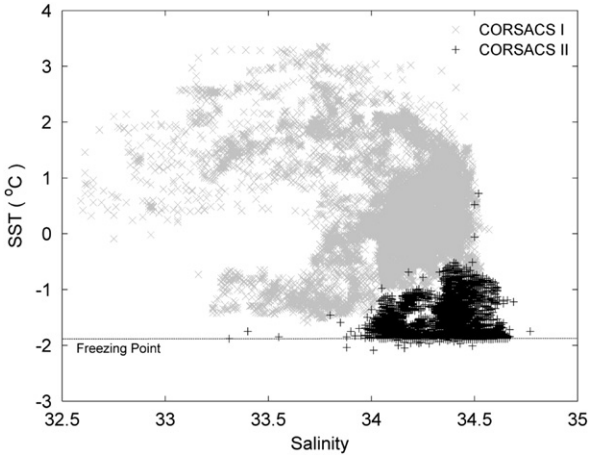

Fig. 2.

34 (mean 34.4 ± 0.14; Figs. 2 and 3). During this cruise, a number of modest salinity excursions (Δsalinity < 0.5) were observed in regions with strong sea ice gradients (*see* Fig. 7). These hydrographic characteristics indicate the presence of recently exposed surface waters following wind-driven ice retreat, with limited *in-situ* ice melting. The lower salinity signal observed in offshore waters (Fig. 4c) likely reflects a limited advection/melting signal in the developing polynya. The median mixed layer depth, computed with a $\Delta\sigma_t$ 0.05 kg m^{-3} criterion, was 90 m during the C2 cruise (± 65 std., range 11–347 m). The variability in mixed layer depths was due in part to a warming of surface waters and increased stratification during our cruise (discussed below).

By comparison with the early season survey, SST and salinity showed substantial variations during the mid-summer C1 cruise (Figs. 2 and 3). SST ranged from ~ −1.5 to 3 °C (mean 0.3 ± 0.8 °C), while salinity ranged from 32.6 to 34.5 (mean 34.2). Ice-melt played a significant role in structuring the spatial variance of upper water column hydrography during this time, as seen by a number of strong salinity gradients (> 1 unit salinity change over < 10 km) associated with rapid changes in ice cover (*see* Fig. 9). High SST, low salinity waters (< 33.5) were most prominent along the Western portion of our survey region (Fig. 4b, d), where ice melt and strong surface warming led to a shallow MLD (~10 m) and strong vertical stratification (Long et al., submitted for publication-b). Lower salinity waters were also observed north of 74°S and were associated with colder waters in the transition through the ice pack into offshore waters (Fig. 4b), likely reflecting an additional ice melt signal. Across the entire summertime polynya, the median mixed layer depth ($\Delta\sigma_t$ 0.05 kg m^{-3}) was 33 m (± 23 std., range 5–178 m).

3.2. Phytoplankton biomass and taxonomic distributions

We used two related variables to estimate phytoplankton biomass in surface waters; Chl *a* concentrations measured at discrete sampling stations, and *in vivo* Chl *a* fluorescence measured with flow-through sensors. For both cruises, there was a strong linear correlation between these variables ($r > 0.7$, $p < 0.001$). However, the slope of the fluorescence vs. Chl *a* relationship for C2 (5.8 ± 0.19) was significantly lower than for C1 (8.4 ± 0.41), indicating lower fluorescence yields per unit Chl *a* in the early season phytoplankton assemblages (*t*-test, $p < 0.001$, df = 906). This result is likely related to differences in photophysiological properties of the early and later season phytoplankton

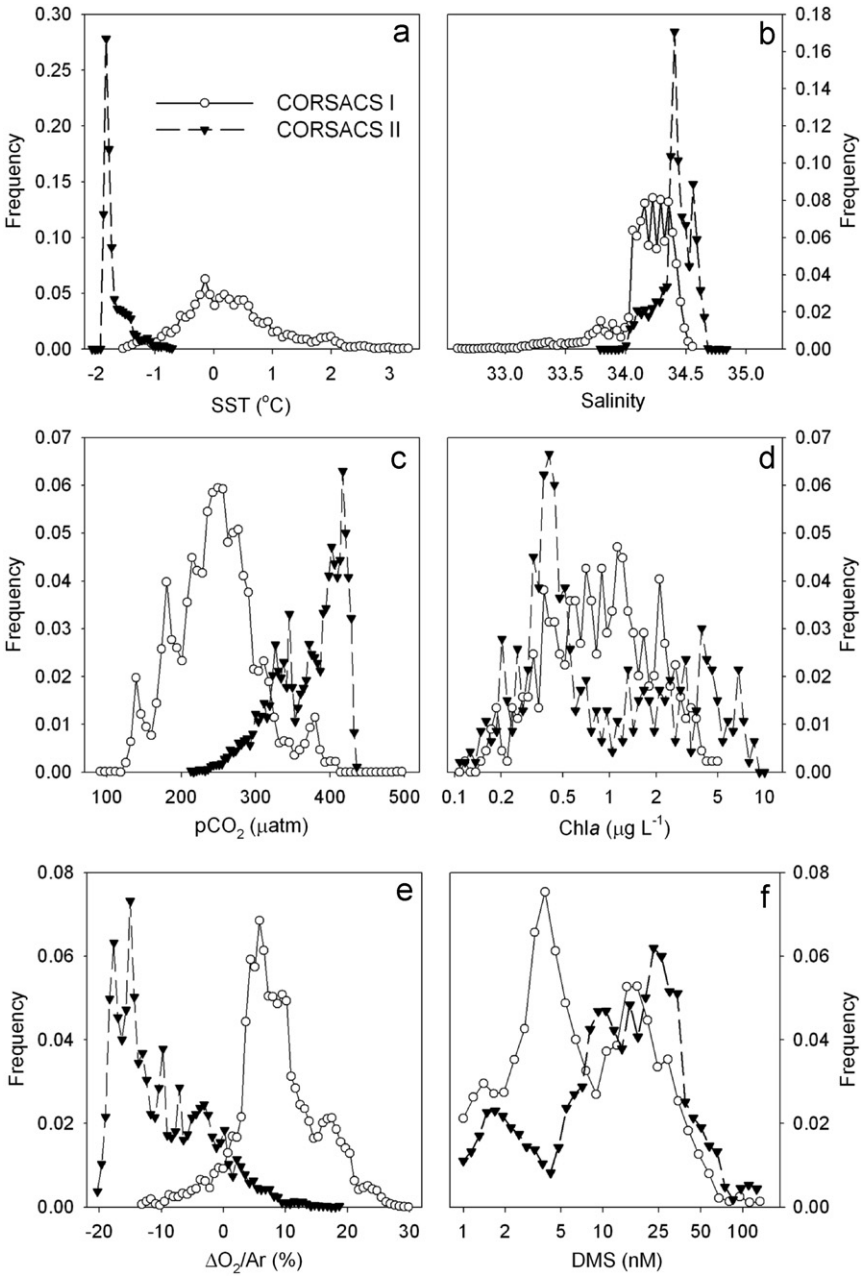

Fig. 3.

assemblages (*see* Section 4). Notwithstanding this seasonal difference, underway Chl *a* fluorescence data provide valuable information on the fine-scale distribution of phytoplankton biomass along our survey transects, and are used below to help interpret underway gas measurements.

During the early season C2 survey, the mean HPLC-derived Chl *a* concentration across our survey region was 1.6 $\mu g\,L^{-1}$ (± 1.9), ranging from 0.2 to 12.2 $\mu g\,L^{-1}$. The frequency distribution of surface Chl *a* fluorescence (Fig. 3d) was distinctly bi-modal. Low Chl *a* fluorescence was observed in ice covered and recently exposed waters north of ~76°S, while high values were observed in the southern and central polynya where waters had been ice-free longest (Fig. 4e). A comparable trend in temporal phytoplankton biomass was also evident in satellite imagery. Areally integrated Chl *a* concentrations (derived from SeaWiFS 8-day composites; http://oceancolor.gsfc.nasa.gov/cgi/l3) increased by ~15-fold across the polynya during our ~3 week occupation (from 0.2 to 2.7 $\mu g\,L^{-1}$), in conjunction with a strong decrease in sea ice cover (Long et al., submitted for publication-b).

During the mid-summer C1 survey, the mean surface water Chl *a* concentration ($1.1 \pm 0.9\ \mu g\,L^{-1}$) was similar to that observed during early spring. However, the range of values was significantly smaller (0.1 to ~5 $\mu g\,L^{-1}$) and Chl *a* fluorescence data followed a log-normal distribution (Fig. 3d). High surface Chl *a* fluorescence was observed in the low salinity waters of Terra Nova Bay (NW polynya), along the northern edge of the Ross Ice shelf west of 180° and in the NE quadrant of the polynya (Fig. 4f). In comparison to the early season cruise, there were smaller temporal changes in surface Chl *a* concentrations during the C1 survey. SeaWiFS-derived areally integrated Chl *a*, (averaged over the entire polynya) decreased by a factor of ~2 during the cruise, indicating that we sampled during the initial declining phase of the phytoplankton bloom.

As expected, we observed significant differences in the taxonomic composition of early vs. mid-season phytoplankton

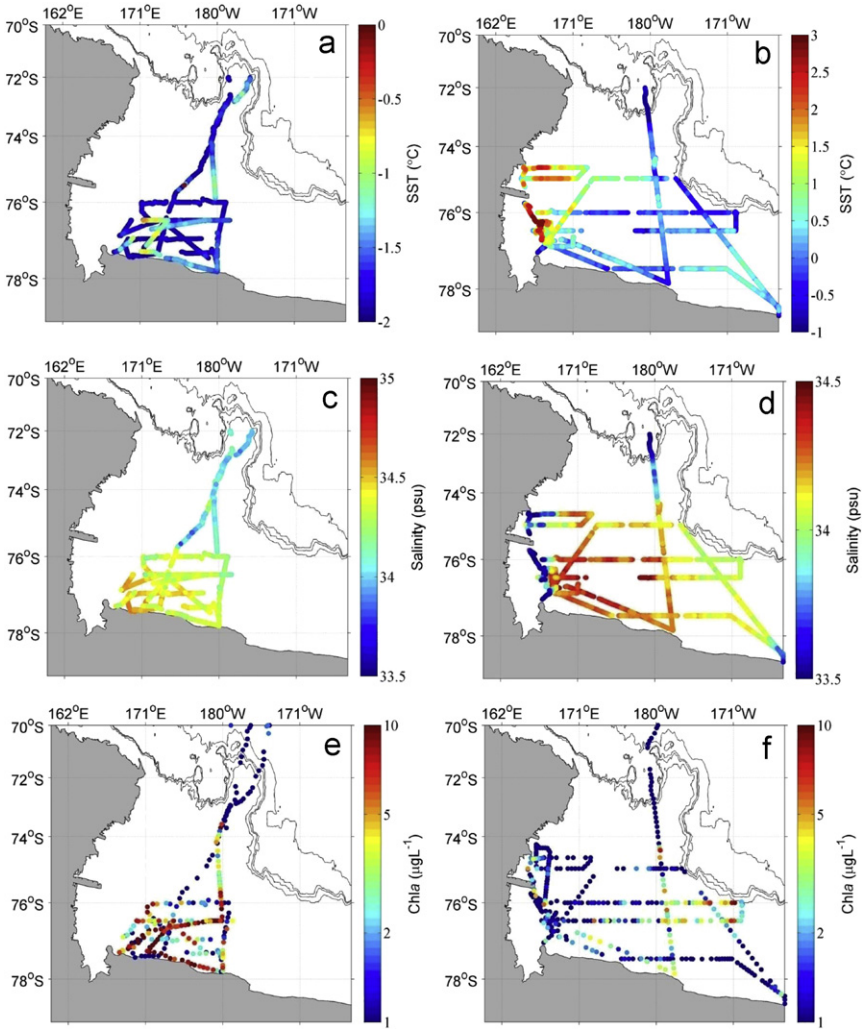

Fig. 4.

assemblages. During our early season C2 survey, colonial *Phaeocystis*-dominated surface waters across nearly all of the polynya south of 76°S, comprising >90% of the total phytoplankton assemblage at many sampling stations (Fig. 5). *Phaeocystis* abundance was significantly lower north of 76°S in regions with increased ice cover, and south of 76°N along the 180° meridian. Phytoplankton taxonomic distributions were more variable in the later season polynya. In general, there was greater diatom prevalence during the C1 cruise, particularly in the highly stratified western sector (*e.g.* Terra Nova Bay) where diatoms accounted for >80% of phytoplankton surface biomass in many areas (Fig. 5). The highest relative *Phaeocystis* abundances during the mid-summer survey were observed in the NE portion of the polynya, and along parts of the Ross Ice Shelf. Mixed diatom/*Phaeocystis* communities appeared throughout the southern/central region.

3.3. Surface water pCO_2 and $\Delta O_2/Ar$

Frequency distribution plots of pCO_2 and biological O_2 saturation ($\Delta O_2/Ar$) (Fig. 3c, e) clearly show the transition from a net heterotrophic system during the early growth season survey (C2) to a net autotrophic summertime regime (C1). At the beginning of our spring-time survey, pCO_2 values generally exceeded atmospheric saturation, while $\Delta O_2/Ar$ was significantly undersaturated across most of the polynya (Fig. 3c, e). This CO_2 supersaturation of surface waters resulted in mean CO_2 efflux to the overlying atmosphere of 4.9 ± 10.6 mmol m^{-2} d^{-1} (range: -9.7 to 28.3). The large range is due to the significant spatial/temporal variability of surface water pCO_2, ice cover and wind speeds encountered during the C2 cruise. The corresponding mean O_2 flux during the C2 survey was -139 ± 215 mmol m^{-2} d^{-1} (range -1321 to 165 mmol m^{-2} d^{-1}), indicating significant net invasion of O_2 into the undersaturated surface waters. Given the high degree of residual O_2 undersaturation, O_2 flux data cannot be used to infer rates of NCP using a steady-state, mixed layer mass balance approach (Reuer et al., 2007).

In contrast to the early spring survey, pCO_2 was well below atmospheric saturation across most of the mid-summer (C1) polynya (mean=246 ± 54 μatm, minimum ~100 μatm), and $\Delta O_2/Ar$ was supersaturated by as much as 30% (mean=+8.6%). During this later season survey, the Ross Sea polynya acted as an overall net CO_2 sink, with a mean daily CO_2 influx of -13.1 ± 9.4 mmol m^{-2} d^{-1} (range: -36.0 to -1.7). Due to relatively constant wind speeds (6.3 ± 2.8 m s^{-1}) and uniformly low sea ice coverage (Fig. 1b), the fluctuations in summer sea-air CO_2 exchange were mostly driven by spatial variability in surface water pCO_2. Mean O_2 fluxes during the summer cruise were 52.2 ± 58.3 mmol m^{-2} d^{-1} (range -222 to 343 mmol m^{-2} d^{-1}).

As discussed above for Chl *a*, much of the apparent variability in pCO_2 and O_2/Ar during the early season C2 cruise reflected the temporal evolution of surface water biogeochemistry rather than

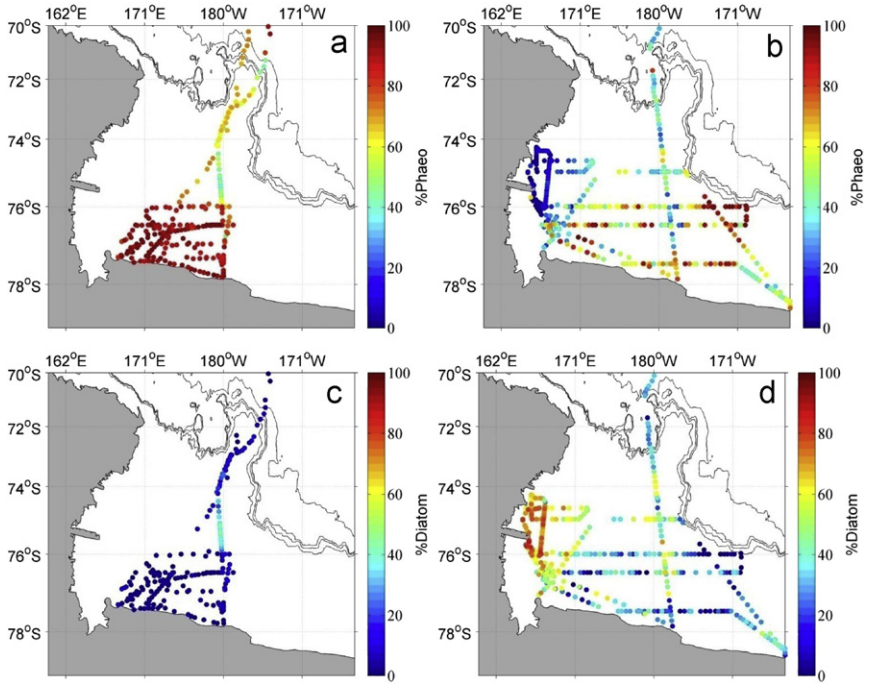

Fig. 5.

spatial patterns *per se*. Maximum pCO_2 undersaturation and $\Delta O_2/Ar$ supersaturation during this cruise were observed in the central polynya (Fig. 6a, c), where surface waters had been ice free longest and phytoplankton blooms were most developed. The temporal dynamics of early season CO_2 and $\Delta O_2/Ar$ distributions are evident in Fig. 7 where underway gas data are plotted versus time (and cruise track distance). All measurements between ~500 and 4000 km along the C2 cruise track were obtained within the polynya, while data collected outside of these ranges are from the ship's transit through sea ice to/from New Zealand. During the initial ~10 days of the early season survey (before ~November 21), there were no clear temporal trends in surface water O_2/Ar or pCO_2. We did, however, encounter several localized regions of significant pCO_2 drawdown, O_2/Ar accumulation and increased Chl *a* (*e.g.* ~500 and 1100 km along the cruise track; Fig. 7a–c). These small-scale features were associated with regions of ice retreat and, in one case (~500 km along the cruise track), a sharp salinity and temperature gradient. During the last week of November and into early December, pCO_2 values fell steadily across the polynya, reaching minimum values of ~200 μatm (Fig. 7b). This pCO_2 drawdown was coincident with a large and rapid increase in Chl *a* fluorescence (Fig. 7a) and $\Delta O_2/Ar$ accumulation to values of ~10% supersaturation (Fig. 7c). The most intense phase of the CO_2 drawdown (after November 26) corresponded to an extended period of ice-free water in our sampling region. During this time, surface water pCO_2 decreased by over 20 $\mu atm\,d^{-1}$, while $\Delta O_2/Ar$ increased by ~3% d^{-1}.

As shown in Fig. 8, increased productivity across the early spring polynya was coupled to a warming of surface waters. Temperature increased by ~0.1 °C d^{-1} during the period of maximum pCO_2 drawdown (O_2/Ar accumulation). This warming was, in turn, associated with decreasing wind speeds ($-0.5\ m\ s^{-1}\ d^{-1}$) and sea ice cover, leading to increased stratification of the mixed layer. MLDs (computed with a density difference criterion—$\Delta_\sigma = 0.05\ kg\ m^{-3}$) decreased by $\sim 5 \pm 3\ m\ d^{-1}$ during the latter phases of our survey (Long et al., submitted for publication-b). This stratification, combined with increasing photoperiod, led to higher integrated irradiance levels more favorable to phytoplankton growth. Given the strong increase in productivity associated with mixed layer stratification, it is unlikely that photoinhibition was a significant factor during the early bloom.

In contrast to the early season survey, we did not observe any clear temporal trends in pCO_2 and O_2/Ar during the summertime C1 cruise (Fig. 9). Rather, spatial heterogeneity dominated the gas distributions during this time. A large seasonally integrated NCP signal, as reflected in low pCO_2, high $\Delta O_2/Ar$ and high Chl *a* was observed across much of the polynya, particularly in the southern and western portion of our survey region (Figs. 4f, 6b, d). The exception to this was a region north of 74°S where ice cover was significant. In this region, pCO_2 exceeded atmospheric equilibrium and $\Delta O_2/Ar$ was undersaturated by up to ~10%, reflecting a net heterotrophic signal under sea ice. In many cases, large changes in mid-summer pCO_2 and O_2/Ar were associated with fine-scale changes in sea ice cover and salinity (*e.g.* ~2600 km along the cruise track; see Fig. 9). These features illustrate the importance of ice melt-derived stratification in driving local productivity gradients. Small-scale variability in pCO_2 and $\Delta O_2/Ar$ was also observed, however, in the absence of sea ice cover. Fig. 10 illustrates the large spatial gradients we observed in summertime gas concentrations in ice-free waters.

Fig. 10 also highlights the strong covariation of pCO_2, $\Delta O_2/Ar$ and Chl *a* we observed in surface waters. Indeed, there was very strong negative correlation between O_2/Ar and pCO_2 across the entire polynya for both the C1 and C2 cruises (Tables 1 and 2). However, the strength of the correlation, and the slope of the O_2/Ar–CO_2 regression line were significantly higher during the early growing season (Fig. 11a). This seasonal difference in slope is even more apparent when pCO_2 and $\Delta O_2/Ar$ are converted to DIC and O_2 concentrations (Fig. 11b). During C1, the O_2 vs. DIC relationship was consistent with the expected photosynthetic stoichiometry (170:117). During C2, however, polynya surface waters exhibited a much greater change in O_2 per unit DIC change, *i.e.* higher O_2 accumulation relative to DIC drawdown. Moreover, there was significantly less scatter in the O_2 vs. DIC relationship in the C2 dataset, indicating a much tighter C–O coupling in the early spring polynya. Similarly, Chl *a*

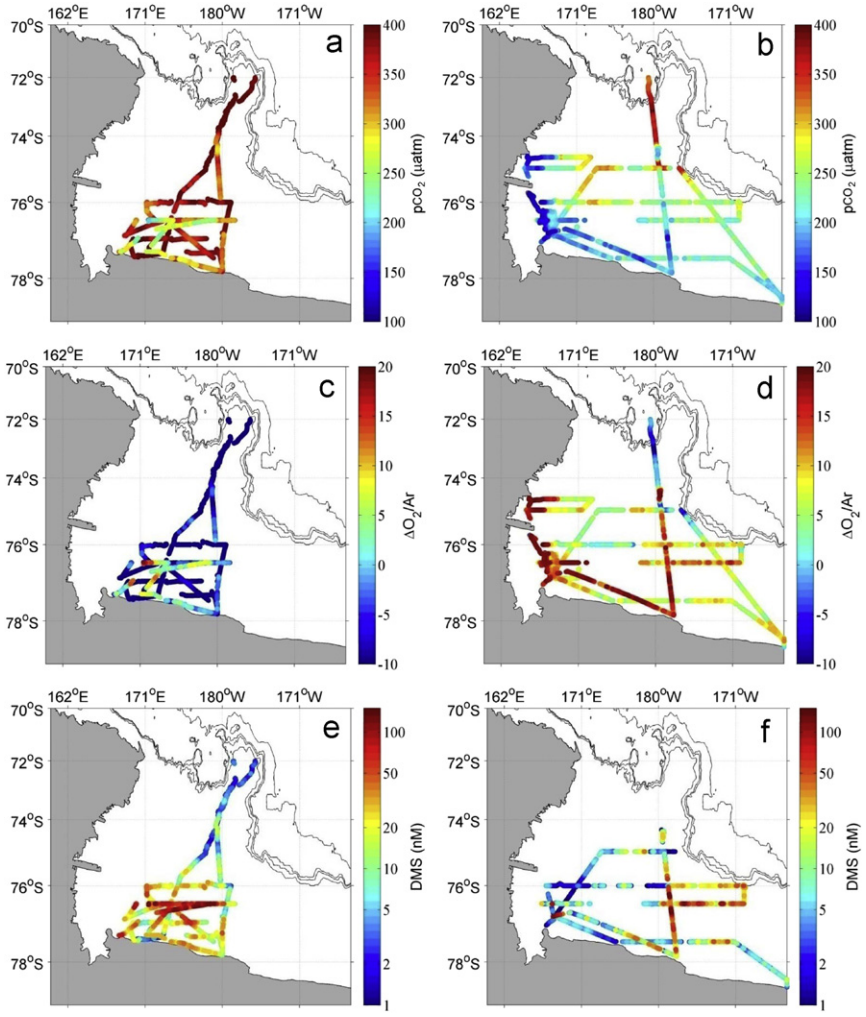

Fig. 6.

concentrations also showed a stronger correlation with O_2/Ar and pCO_2 during the early season cruise (Tables 1 and 2).

3.4. DMS distributions

Comparison of the MIMS-based underway DMS measurements with purge and trap Gas Chromatographic (GC) data from 5 m Niskin bottle samples (P. Lee and G. DiTullio, unpublished data) showed good consistency between methods. Pearson correlation coefficients (r) in the regression of MIMS-DMS vs. GC-DMS were 0.93 and 0.95 for C1 and C2, respectively (data not shown). However, there was an offset in the absolute concentrations measured by these methods. On average, MIMS measurements were lower than GC measurements during the C1 cruise (regression slope $=0.75\pm0.05$), and higher than GC measurements during C2 (slope 1.22 ± 0.07). Perfect agreement is not expected between these measurements given the difference in sampling methods (*i.e.* Niskin bottles vs. the ship's seawater supply line) and the high degree of small-scale patchiness observed in surface DMS distributions. There have been recent suggestions that exact DMS concentrations may be subject to some uncertainty due to sample handling artifacts that may cause the lysis of *Phaeocystis* colonies and subsequent release of DMS (del Valle et al., 2009). Our MIMS-based measurements do not require the manipulation and handling of discrete water samples, but it is possible that cell lysis occurs in the ship's seawater supply system, or in the pump we use to deliver water through our sampling cuvette. This would be particularly problematic during the C2 cruise when colonial *Phaeocystis* was most abundant, and it may explain why MIMS-based DMS concentrations were higher than conventional GC-based measurements during the early season cruise. The lower DMS values obtained by MIMS relative to GC during the summertime cruise are more difficult to explain, and may be related to offsets in the primary standards used to calibrate GC and MIMS measurements. Notwithstanding some degree of uncertainty in the absolute MIMS-based DMS concentrations, the absolute discrepancy between GC and MIMS data is small compared to the observed DMS variability, and it does not alter the main conclusions we draw from our results.

Across our two surveys, DMS concentrations (based on MIMS) ranged from below detection limit ($<\sim1$ nmol L^{-1}) to ~150 nmol L^{-1}. Average DMS concentrations during the early season survey (19 ± 19 nmol L^{-1}) were $\sim$2-fold higher than mean concentrations during the later season (8.7 ± 13 nmol L^{-1}). Higher early season DMS concentrations, coupled with greater mean wind speeds led to $\sim$2-fold higher sea-air fluxes during C2, despite significantly greater sea ice cover. Mean sea-air DMS fluxes across our sampling region were 0.04 ± 0.03 and 0.02 ± 0.02 mmol m^{-2} d^{-1} for C2 and C1, respectively.

During the early season survey, the spatial distribution of DMS was influenced by the temporal dynamics of bloom development

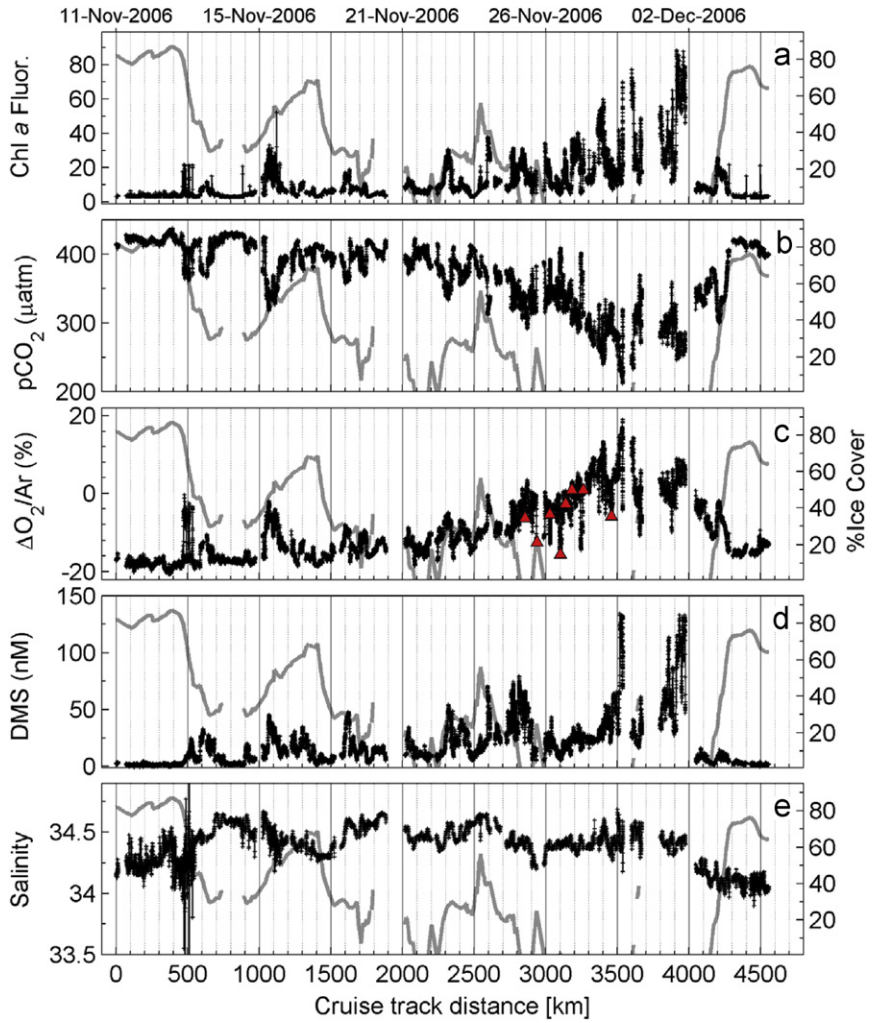

Fig. 7.

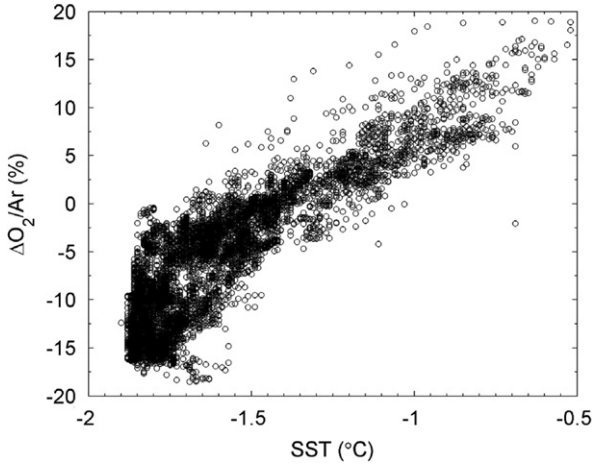

Fig. 8.

(Fig. 7). The highest concentrations were observed in the central polynya which was sampled several weeks after ice retreat, while low concentrations were observed during the early phase of our survey in recently ice-free waters (Fig. 6e). During the later season C1 survey, maximum DMS levels were observed in the central and eastern portions of the polynya, while lower concentrations were observed in the highly productive waters of the southwestern polynya (Fig. 6f). Due to detector problems, DMS data are not available for the northwest region of the C1 survey (near Terra Nova Bay). For both cruises, low DMS concentrations (<10 nmol L^{-1}) were found in the northern polynya (*i.e.* north of $\sim$76°S), while high DMS levels were consistently observed along portions of the Ross Ice Shelf (Fig. 6e, f).

We observed significant small-scale patchiness in surface water DMS distributions during both the early and later season surveys. Several examples of this are shown in Fig. 10, where DMS concentrations change by >50 nM on scales $\ll 10$ km. In some cases (*e.g.* $\sim$3500 km along the C2 cruise track; Fig. 7d), large DMS excursions were related to fine-scale productivity gradients as reflected in CO_2, O_2/Ar and Chl *a* fluorescence signals. In other cases (*e.g.* $\sim$2600 km along the C1 cruise track; Fig. 10d), DMS levels remained nearly constant despite large changes in other gases and hydrographic variables.

During the early spring cruise, DMS concentrations were strongly correlated to pCO_2 O_2/Ar and Chl *a* (Table 1), suggesting a relationship with bulk primary productivity across the polyna. In contrast, DMS was only weakly correlated to these variables during the later season survey (Table 2). For C1, where phytoplankton taxonomic variability was greatest, high DMS concentrations were observed in regions dominated by both diatoms and *Phaeocystis* (compare Figs. 5 and 6f), and there was no apparent correlation between DMS levels and the relative or absolute abundance of diatoms or *Phaeocystis* measured along the cruise

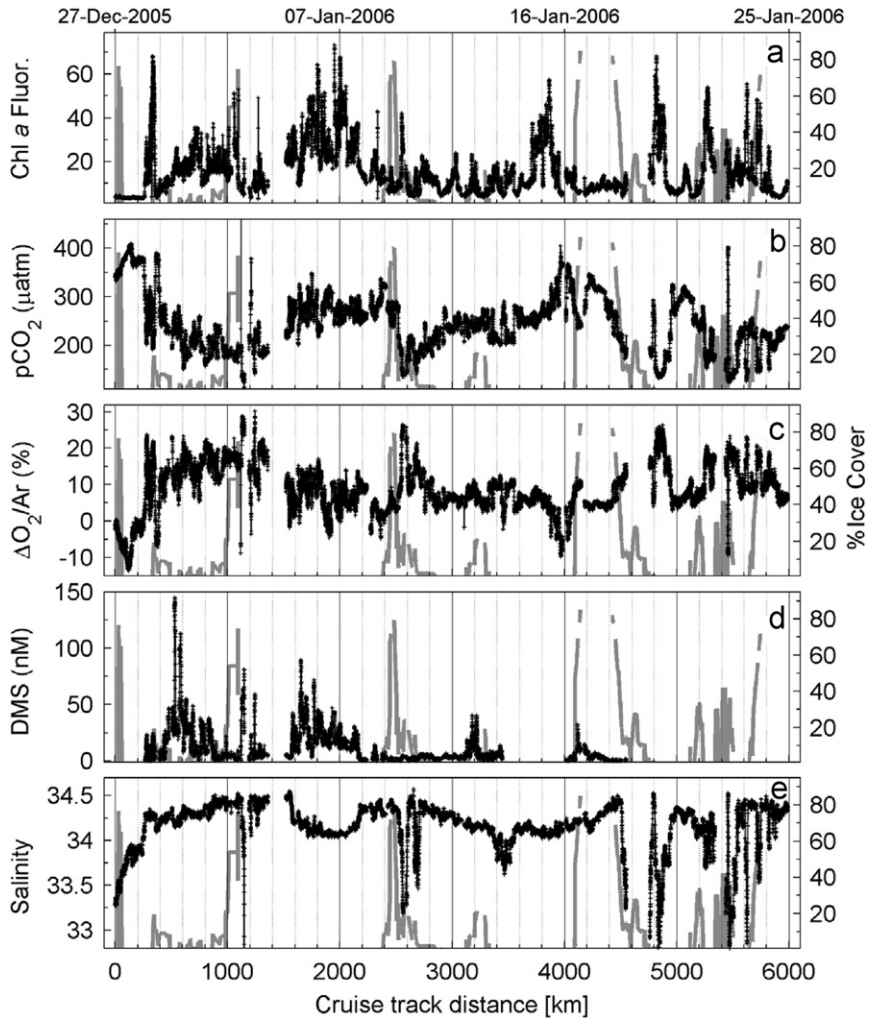

Fig. 9.

track ($r < 0.15$; data not shown). In contrast, DMS concentrations were strongly correlated ($r = 0.71$) with absolute *Phaeocystis* abundance during the C2 survey.

3.5. Length scales of variability

Fig. 12 shows an example of computed interpolation errors for one of the 5 transects we examined. Characteristic length scales of variability (x_{char}) were similar for all variables, ranging from ~8 to 15 km (Table 3). This length scale corresponds to the distance below which most of the spatial variability is observed, and the values we obtained were consistent with that reported by Hales and Takahashi (2004) in previous Ross Sea surveys of O_2, pCO_2, salinity and temperature. The absolute value of the maximum interpolation error (E_∞) varied strongly across the variables we measured (Table 3). Errors were small for temperature and salinity (which showed the smallest absolute variability across our transects), but much larger for Chl *a* and gases. Given the relatively small number of transects we analyzed, we could not quantitatively examine differences in spatial variability between the two cruises.

4. Discussion

Our results document, with high resolution, spatial and temporal heterogeneity in mixed layer gas concentrations that is generated by coupled physical/biological processes. The early season (C2) cruise captured the winter – spring transition, during the time of rapid ice retreat and phytoplankton bloom initiation, when the Ross Sea is clearly a non-steady-state system. These early season blooms impart a *de novo* biogeochemical signature on Ross Sea surface waters, since winter convection effectively resets the water column and erases the imprint of biological productivity from the previous growth season (Gordon et al., 2000). In contrast, the C1 summer cruise occurred after the peak of primary productivity in the polynya, when temporal changes in phytoplankton biomass were relatively low, and the system approaches a steady state in terms of gas fluxes. Gas distributions during this later season period reflect both instantaneous productivity and a cumulative biogeochemical signal that is influenced by mixing and air-sea exchange (Long et al., submitted for publication-a, submitted for publication-b). Below, we discuss our results in the context of these controlling factors.

4.1. Early spring pCO_2 and O_2/Ar

Early season polynya waters sampled shortly after sea ice retreat exhibit significant pCO_2 supersaturation and O_2/Ar undersaturation, reflecting deep winter mixing and net heterotrophy. Following the initial retreat of sea ice, both gas exchange and NCP act to drive gas concentrations towards atmospheric equilibrium,

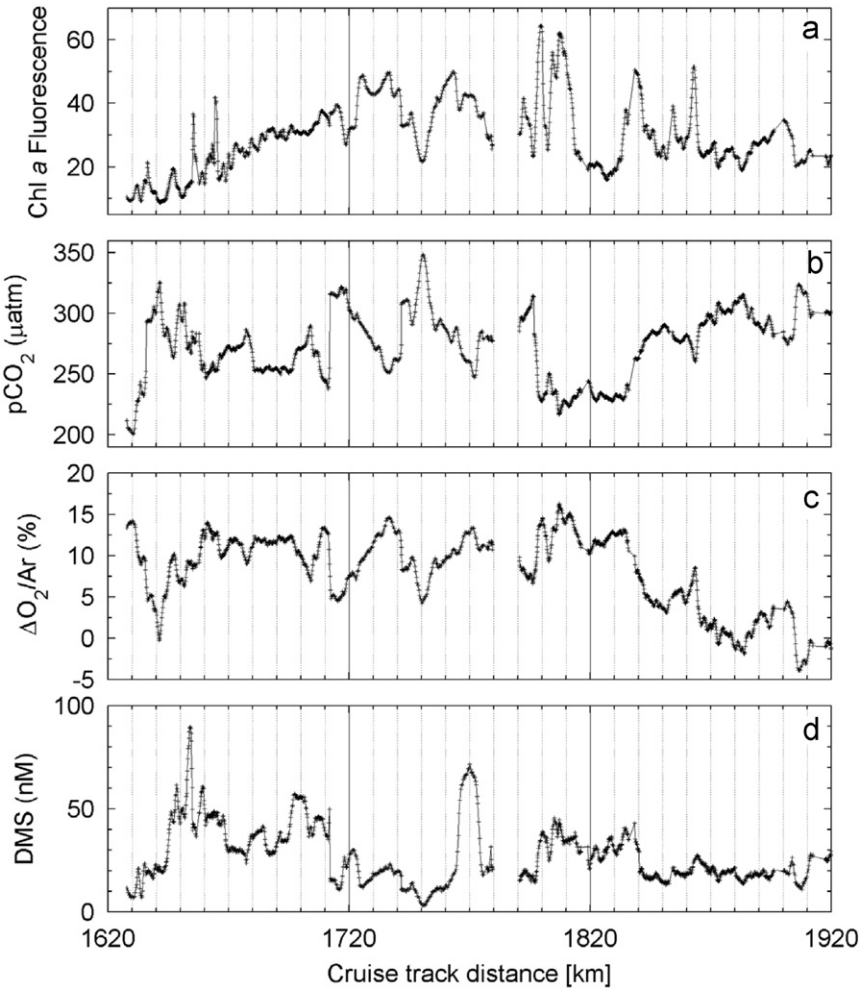

Fig. 10.

Table 1
Correlation coefficients between underway measured parameters during the CORSACS II (spring-time survey).

	DMS	Chl *a* fluor.	$\Delta O_2/Ar$	pCO_2	Salinity	SST
DMS	1.00					
Chl *a* fluor.	0.75	1.00				
$\Delta O_2/Ar$	0.69	0.78	1.00			
pCO_2	−0.73	−0.81	−0.98	1.00		
Salinity	0.25	0.12	0.08	−0.06	1.00	
SST	0.39	0.50	0.79	−0.76	−0.19	1.00

Table 2
Correlation coefficients between underway measured parameters during the CORSACS I (mid-summer) survey.

	DMS	Chl *a* fluor.	$\Delta O_2/Ar$	pCO_2	Salinity	SST
DMS	1.00					
Chl *a* fluor.	0.34	1.00				
$\Delta O_2/Ar$	0.22	0.33	1.00			
pCO_2	−0.03	−0.21	−0.88	1.00		
Salinity	−0.18	−0.14	−0.12	0.15	1.00	
SST	−0.09	−0.07	0.45	−0.42	−0.12	

and the polynya exhibits clear non-steady-state dynamics. The efficiency of gas exchange depends on wind-speed, ice cover and MLD, which can change rapidly over both space and time during the early spring bloom. Moreover, ice cover and mixing depth control the mean irradiance experienced by phytoplankton and thus strongly influence NCP (Arrigo et al., 1998a). We used a simple box model to explore the sensitivity of surface water pCO_2 and $\Delta O_2/Ar$ to ice-dependent gas exchange, MLD and NCP. Fig. 13 shows the calculated effect of MLD on the evolution of surface water pCO_2 and $\Delta O_2/Ar$ with and without NCP (100 mmol O_2 m^{-2} d^{-1}). Irrespective of biological production, decreasing MLD increases the efficiency of gas exchange since there is a smaller volume of water exchanging with the atmosphere. Since air-sea exchange of O_2 occurs far more rapidly than for CO_2, the temporal evolution of $\Delta O_2/Ar$ shows a strong MLD dependence, whereas pCO_2 does not. During the initial 'pre-bloom' phase (days 0–8 on Fig. 13), the observed time course of $\Delta O_2/Ar$ is consistent with generally deep mixed layers (*i.e.* >100 m) since shallow mixed layers (*e.g.* 25 m) produce a time course of $\Delta O_2/Ar$ equilibration that is much faster than observed. In contrast, the observed time course of $\Delta O_2/Ar$ during the bloom initiation phase (after day 10), can only be reproduced with significantly shallower MLD (*i.e.* $\ll 100$ m). This analysis thus suggests that shoaling mixed layers exert an important control on the rate of O_2 accumulation in surface waters during the early spring.

A key result of our analysis is that the MLD effect on the $\Delta O_2/Ar$ re-equilibration time-scale largely dominates over the biological production signal during the early spring bloom under conditions of O_2 undersaturation. Even the high rates of NCP used in our calculation exert only a small influence on the time course of $\Delta O_2/Ar$,

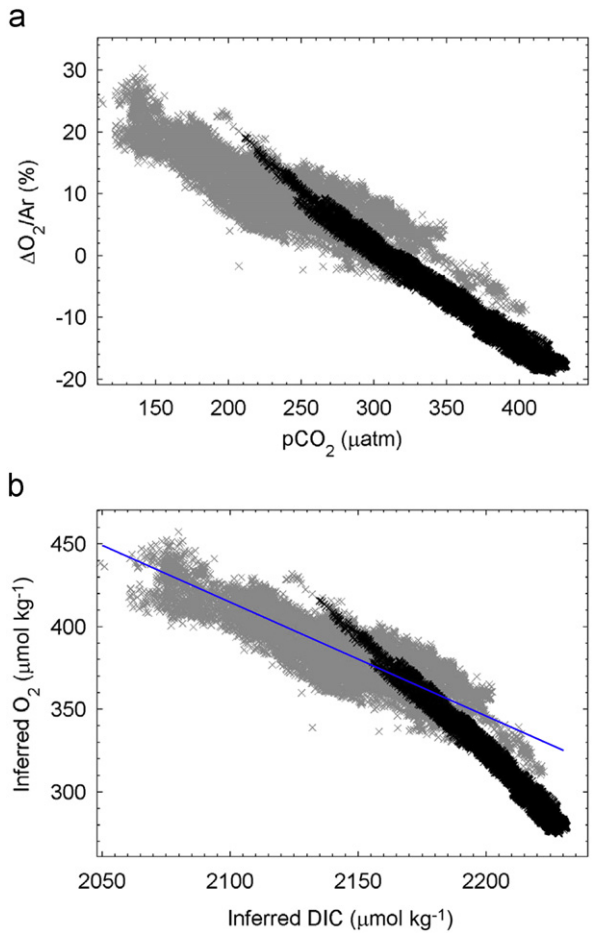

Fig. 11.

particularly under conditions of deep mixing (compare solid and dashed lines in Fig. 13). Under these early season, non-steady-state conditions, gas exchange thus exerts a primary control on mixed layer $\Delta O_2/Ar$. However, a biological imprint on $\Delta O_2/Ar$ is apparent towards the end of our survey ($\sim$day 18) after O_2 reaches atmospheric saturation ($\Delta O_2/Ar=0$). After this equilibrium point is achieved, NCP is the only process that can yield O_2/Ar supersaturation, while gas exchange acts to reduce O_2 accumulation in the mixed layer above its equilibrium value. Thus, gas exchange and NCP act in opposition to move the system closer to a steady-state balance.

Since gas exchange is comparatively sluggish for CO_2, biological processes exert a larger role in driving mixed layer concentrations than they do for O_2. This can be seen in Fig. 13c, d, where gas exchange alone (*i.e.* NCP=0, solid lines on figure), cannot reproduce the observed evolution of surface water pCO_2, even with a shallow mixed layer. Rather, the combination of NCP and MLD dictate the magnitude of pCO_2 drawdown, with increasing integrated drawdown per unit NCP at shallower MLD. This coupled NCP–MLD effect is illustrated in Fig. 14 which shows the rate of pCO_2 drawdown in the mixed layer (estimated from a regression of the log-transformed pCO_2 time-course data) as a function of these two variables. The thick black line plotted on the figure represents the observed rate of mixed layer pCO_2 drawdown during the bloom phase (days 10–18; $\sim$11 ppm d^{-1}). In our simulation, this pCO_2 drawdown is obtained over a range of NCP from 30 to 140 mmol C m^{-2} d^{-1} and MLD of 5–30 m. Values on the upper end of the NCP range and lower end of the MLD range are not likely observed in the Ross Sea.

The analysis described above uses the daily mean wind speeds and sea ice cover observed during our survey to drive air-sea exchange parameterizations. We can, however, use our box model to examine the sensitivity of mixed layer pCO_2 and $\Delta O_2/Ar$ dynamics to the range of sea ice and wind conditions. Given the weak contribution of gas exchange to the CO_2 mass balance, these variables have little effect on mixed layer pCO_2 dynamics. Assuming a 100 m mixed layer with 50 mmol m^{-2} d^{-1} NCP and wind speeds ranging from 5 to 20 m s^{-1}, there is no significant effect of ice cover on surface pCO_2 over 10 days. In contrast, ice cover exerts a much stronger influence on the trajectory of mixed layer $\Delta O_2/Ar$. For example, at high wind speeds (20 m s^{-1}), we calculate an increase of 9% in biological O_2 saturation in the absence of sea ice relative to 75% ice cover. This result applies under conditions of O_2 undersaturation, where the presence of sea ice acts to limit the equilibration of $\Delta O_2/Ar$ with the overlying atmosphere. In a situation of strong net O_2 production in ice-covered waters, the presence of sea ice would act to increase the accumulation of photosynthetically derived O_2 in surface waters. These calculations are based on a simple parameterization of the sea-ice dependence of air-sea fluxes (inversely proportionately to the fractional ice cover) which are still subject to significant uncertainty. Nonetheless, our box model results clearly show the much greater sensitivity of mixed layer $\Delta O_2/Ar$ to wind speed and sea ice cover.

Beyond the broad-scale evolution of pCO_2 and $\Delta O_2/Ar$ that is driven by NCP, gas exchange and shoaling mixed layers, the observed $\Delta O_2/Ar$ and pCO_2 distributions show a number of small-scale features that deviate from the mean secular trend. This small-scale variability reflects the convolution of spatial and temporal heterogeneity in the early season polynya. Our data were collected from a moving platform, and thus incorporate significant variance due to spatial heterogeneity that is manifest as excursions from the mean temporal evolution of the system. Based on the analysis presented above, we can infer the nature of the physical-biological mechanisms forcing these small-scale excursions. Regions where both $\Delta O_2/Ar$ is high and pCO_2 is low must have relatively shallow MLDs and/or greater NCP. Conversely, low $\Delta O_2/Ar$ and high pCO_2 reflect more deeply mixed, less productive regions, perhaps influenced by localized vertical entrainment of deep water. Although we did not include entrainment fluxes in our box model calculations, we found a clear negative correlation between MLD and $\Delta O_2/Ar$ for the early spring cruise ($\Delta O_2/Ar = -3.9 \times MLD - 0.077$, $r=0.59$). Since surface macronutrients were replete during the spring cruise, NCP was likely stimulated by enhanced light availability and/or micronutrient enrichment, which are in turn, tied to MLD dynamics. The physical mechanisms forcing short-length-scale variability in MLD may include sub-mesoscale restratification (Long et al., submitted for publication-a) or localized ice melt contributions. These processes are discussed further in Section 4.4.

4.2. Summertime pCO_2 and O_2/Ar distributions

Net primary productivity in the Ross Sea remains high throughout the summer months, well beyond the early spring bloom period. This persistent high productivity is fueled by abundant macronutrients and enhanced vertical stratification associated with surface warming and ice melt. In localized ice-melt regions, we observed $\Delta O_2/Ar$ values approaching 30% above atmospheric equilibrium, indicative of highly favorable conditions for intense biological production. In addition to its affects on surface buoyancy and vertical stratification, ice melt has also been suggested as a potential source of Fe (Sedwick and DiTullio, 1997) which has been suggested as an important limiting factor for

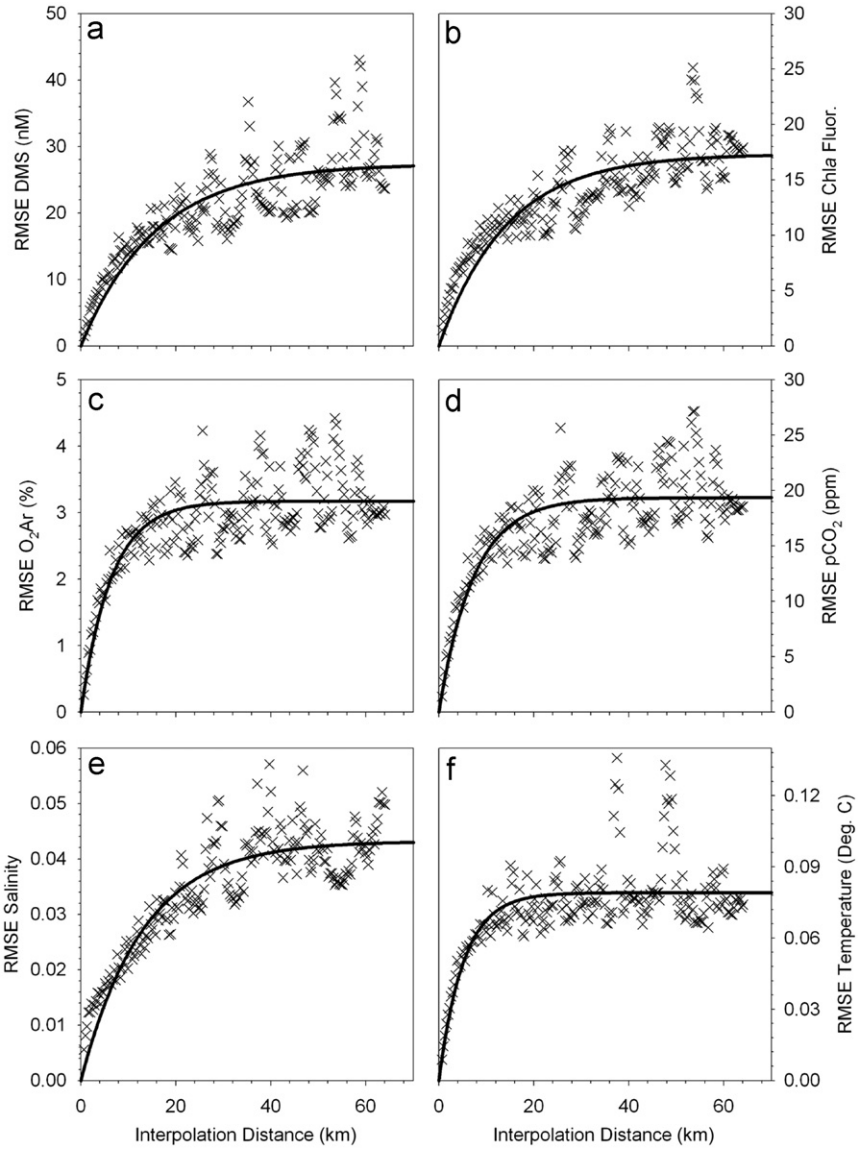

Fig. 12.

Table 3
Computed length scales of variability based on interpolation analysis.

	Length scale, χ_{char} (km)	Asymptotic error
DMS	14.5 ± 3.4	11.1 ± 4.0 (nM)
Chl *a* fluor.	10.6 ± 1.8	7.3 ± 2.7 (V)
$\Delta O_2/Ar$	9.5 ± 1.9	2.5 ± 0.3 (%)
pCO_2	8.3 ± 1.2	16.1 ± 1.2 (matm)
Salinity	10.5 ± 1.3	0.1 ± 0.02 (psu)
SST	12.0 ± 4.8	$0.2 \pm .05$ (°C)

$N=5$, std. error presented.

summertime productivity in the Ross Sea (Coale et al., 2003; Sedwick et al., 2000). During our C1 survey, however, there was limited evidence of an ice effect on surface dissolved Fe levels (Sedwick et al., submitted for publication). Thus, high productivity associated with local salinity anomalies (Fig. 9) likely reflected the influence of ice melt on stratification and mean irradiance levels in the mixed layer, rather than Fe fertilization.

Despite high rates of summertime net primary productivity, air-sea fluxes and physical mixing act to decouple variance in mixed layer gas concentrations from variance in active biological processes. This uncoupling is reflected in the weak correlation between $\Delta O_2/Ar$ and phytoplankton biomass proxies (Chl *a* fluorescence) across the summertime polynya (Table 2). This weak correlation may be partly attributable to the greater variability in Chl *a* fluorescence yields during the summertime cruise, resulting from a larger range of phytoplankton taxonomic composition and mixed layer light regimes across the polynya during the later growth season. Similarly, greater variability in the POC:Chl *a* ratio observed during C1 relative to C2 (Long et al., submitted for publication-a), could contribute to an uncoupling in $\Delta O_2/Ar$ from Ch l*a* (note, however that some of the POC estimates during C1 may include a significant detrital component). It is likely, however, that much of the variability in the Chl *a*–O_2/Ar relationship results from the influence of gas exchanges on surface water O_2 dynamics. As the system approaches steady-state conditions, changes in O_2/Ar per unit NCP decline as sea-air flux acts in opposition to photosynthetic O_2 production in the mixed layer.

As the Ross Sea polynya approaches a steady-state condition, with biological O_2 production balanced by sea-air fluxes, temporal

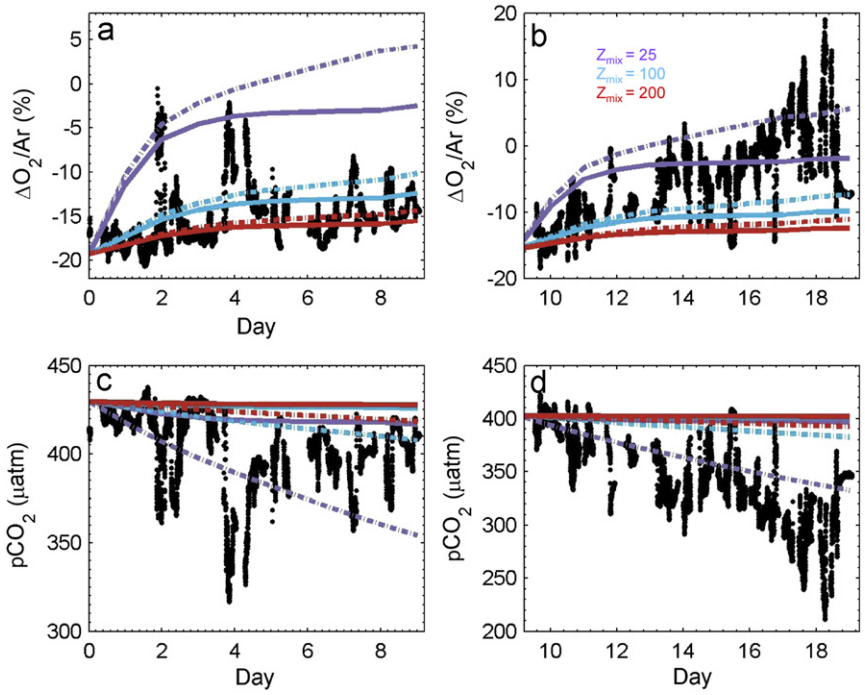

Fig. 13.

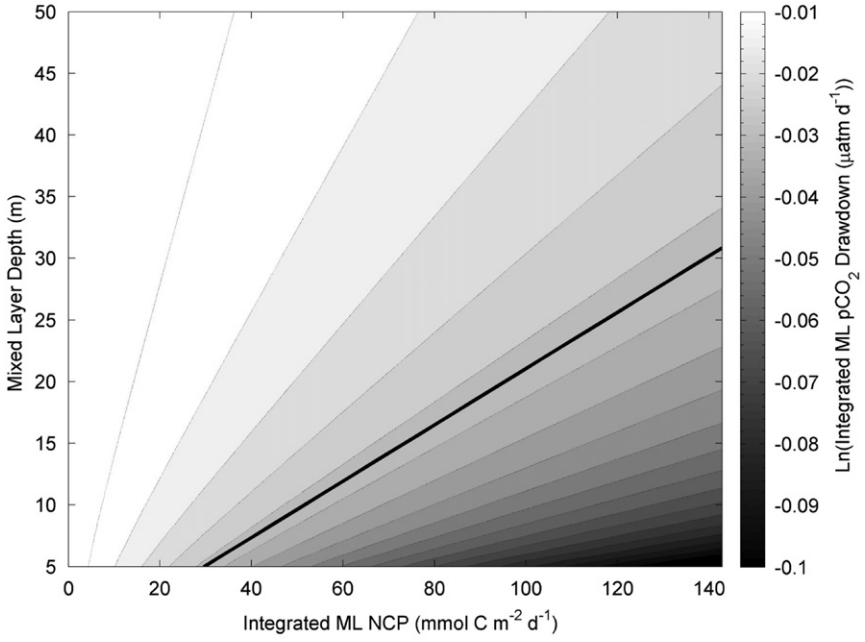

Fig. 14.

variability becomes increasingly dominated by variability in wind speeds. While air-sea gas fluxes clearly influence the summertime pCO_2 and O_2/Ar distributions, differential gas exchange helps explain the reduced correlation between pCO_2 and O_2/Ar observed during the mid-summer cruise, and the seasonal differences in the pCO_2 vs. O_2/Ar slopes (Fig. 11a). The seasonal difference of C–O stoichiometry can be understood more easily when pCO_2 and ΔO_2/Ar data are converted to DIC and O_2, respectively. As shown in Fig. 11b, the overall DIC vs. O_2 slope during the summertime C1 cruise, was consistent with the 170:117 stoichiometry expected for photosynthesis. In contrast, data from the early spring C2 cruise showed a significantly greater rate of O_2 accumulation per unit DIC. While the ratio of CO_2 and O_2 piston velocities changes as a function of temperature due to differential changes in Schmidt numbers for these gases, the effect on gas exchange is minimal ($<1\%$) and cannot account for the change in slope we observe. Rather, this result can be understood in terms of the more rapid gas exchange for O_2 relative to pCO_2, which acts to eliminate disequilibria in O_2 disequilibria faster than for pCO_2. Thus air-sea O_2 exchange with

the highly undersaturated early season surface waters can likely explain much of the difference in C–O slopes between the two cruises.

In addition to differential air-sea gas exchange, seasonal differences in the carbonate system buffering capacity influence the coupling of mixed layer O_2 and CO_2. As pCO_2 drawdown increases, the rate of change of pCO_2 per unit dissolved inorganic carbon drawdown, *i.e.* the Revelle Factor, is reduced (15.3 and 18.2 for C1 and C2, respectively (Long et al., submitted for publication-a). The net result is that biological C drawdown in the early spring produces a correspondingly larger pCO_2 drawdown than during the later summer period. This effect acts to partially offset the influence of differential gas exchange discussed above.

4.3. DMS

Our measurements reveal a clear seasonal difference in DMS concentrations that is consistent with previous reports from the Ross Sea showing elevated spring-time values relative to the later growing season (Kiene et al., 2007). One potential explanation for the higher spring-time DMS concentrations is the increased biomass of *P. antarctica* in phytoplankton assemblages. This species is a prolific producer of the DMS precursor DMSP and has high cellular concentrations of DMSP-lyse (Stefels and Vanboekel, 1993; Stefels and Dijkhuizen, 1996), the enzyme which catalyzes DMSP cleavage to DMS and acrylate. Previous authors have attributed high spring-time DMS concentrations to the abundance of *Phaeocystis* in Ross Sea phytoplankton assemblages (Ditullio and Smith, 1995). In our C2 dataset, we found that surface DMS concentrations were, indeed, tightly coupled to total Chl *a* concentrations and the biomass of *Phaeocystis*. During the C1 cruise, however, we found no correlation between DMS concentrations and the relative or absolute abundance of *Phaeocystis*, suggesting that factors other than phytoplankton taxonomy control surface DMS distributions across the summertime polynya.

Numerous attempts have been made to link phytoplankton taxonomy and production of DMSP to DMS concentrations. Yet due to the complex series of biotic and abiotic interactions and processes linking phytoplankton ecophysiology and DMS/P production and consumption, the exact relationship remains uncertain (Ayers and Cainey, 2007; Stefels et al., 2007). Results from manipulative on-deck experiments conducted during the CORSACS cruises show that changes in light, pCO_2, iron and temperature can have differential and non-linear effects on both phytoplankton taxonomy and intracellular DMSP concentrations (Rose et al., 2009; Feng et al., 2010; P. Lee et al., unpubl. data). Such effects may serve to mask any overall relationship between phytoplankton taxonomy and DMS concentrations.

Given the potentially variable roles of DMS(P) in cellular metabolism, the relationship between phytoplankton biomass and DMS should depend, in part, upon the physiological status of cells. It has been proposed that DMS(P) and DMSO may function as a cellular anti-oxidant system (Sunda et al., 2002) under high light/low Fe/low CO_2 conditions, such that the abundance of these compounds may be related to oxidative stress experienced by phytoplankton. Several lines of evidence suggest that phytoplankton exhibited greater oxidative stress during the later growth season (C1). Higher Chl *a* fluorescence yields during the C1 cruise suggest excess light energy dissipation by phytoplankton. This idea is further supported by accessory photosynthetic pigment data. The two xanthophyll pigments diatoxanthin (DT) and diadinoxanthin (DD) dissipate excess energy through non-radiative pathways, and the DT/DD ratio has been utilized as a measure of non-photochemical quenching (NPQ) by cells (Muller et al., 2001). We observed a higher ratio of diatoxanthin (DT) to diadinoxanthin (DD) in summer phytoplankton assemblages (0.45 and 0.19 for C1 and C2, respectively), suggesting higher NPQ and greater light stress during the summer growth season. According to the hypothesized role of DMS(P) as a cellular anti-oxidant (Sunda et al., 2002), increased light stress would lead to higher summertime DMS production relative to spring time. However, we found no systematic relationship between DMS concentrations and Chl *a* fluorescence yields or DT:DD ratios along either of our survey cruises, suggesting that water column DMS concentrations were not directly related to these physiological variables. This result is indicative of the complex balance of production and consumption terms driving net DMS accumulation (or loss) in the mixed layer.

While our observations provide no information on the rate of dominant DMS production and consumption terms, results from previous studies shed some light on the potential causes for increased spring-time accumulation of DMS in the Ross Sea mixed layer. During the early growth season, DMS accumulation in the mixed layer appears to be coupled to phytoplankton biomass, suggesting a direct production from *Phaeocystis* colonies or indirect bacterial conversion of dissolved DMSP to DMS. Previous field studies suggest that DMS is removed relatively slowly from the Ross Sea mixed layer during the early bloom phase, with photo-oxidation acting as the dominant sink term (Toole et al., 2004), and sea-air fluxes accounting for $\sim$10% of DMS losses. del Valle et al. (2009) have recently argued that a small DMS loss term during the early spring allows the accumulation of high mixed layer DMS concentrations, consistent with our observations during the C2 cruise. As the growing season progresses, rate measurements demonstrate a strong increase in bacterial DMS consumption (BDMSC), likely in conjunction with increased DOC supply through the microbial loop. del Valle et al. (2009) have reported peak summertime BDMSC rates of up to $\sim$8 nmol L^{-1} d^{-1} (equivalent to 0.4 mmol m^{-2} d^{-1} for a homogeneous 50 m mixed layer). These rates yield DMS turnover rates with respect to BDMSC that are at least one order of magnitude greater than sea-air fluxes (mean sea-air flux = 0.02 mmol m^{-2} d^{-1} for the C1 cruise). Such high biological turnover rates would act to limit DMS accumulation in the mixed layer and may partially explain the $\sim$2-fold lower DMS concentrations we observed during the C1 cruise. Moreover, the rapid turnover of DMS in the summertime mixed layer can explain the weak coupling between DMS and phytoplankton biomass (either total chlorophyll *a*, or *Phaeocystis*). During the C1 cruise, 95% of surface DMS concentrations were $<$30 nM, and $\sim$75% were less than 10 nM (Fig. 3f). Given, the rapid biological consumption rates observed during summer, these surface concentrations could turnover on the time scale of several days. This turnover time is significantly faster than that of even rapidly sinking *Phaeocystis* blooms, which may persist in surface waters for several weeks (DiTullio et al., 2000). This discussion highlights the importance of quantifying DMS source/sink terms to understand the dominant factors controlling DMS concentrations in the Ross Sea. In future studies, underway MIMS measurements could be used to identify, in real-time, large gradients and 'hot-spots' of DMS where focused process studies could be conducted. Direct measurements of DMS(P/O) turnover rates, coupled with information on bacterial abundance, productivity and taxonomic composition will provide significant insight into the mechanistic controls on DMS dynamics in marine surface waters.

4.4. Spatial heterogeneity

Over the past 15 years, our understanding of regional biogeochemical cycles in the Ross Sea has increased significantly as a result of several comprehensive field programs including AESOPS and ROAVERRS (Smith and Anderson, 2003; DiTullio and Dunbar, 2003).

By comparison, the processes driving sub-mesoscale variability in this and other oceanic regions remain poorly understood, even though it is now clear that such small-scale variability is pervasive in the oceans (Doney et al., 2003). Our data and those of Hales and Takahashi (2004), demonstrate that much of the variability in gas distributions in the Ross Sea is concentrated at scales (<20 km) that are well below the sampling resolution of typical hydrographic surveys. Our interpolation analysis (Fig. 12) provides estimates for the expected error associated with low resolution sampling. For physical variables such as SST and salinity, these errors are largely insignificant for most biogeochemical calculations, as discussed by Hales and Takahashi (2004). However, the estimation errors associated with the measured gases and Chl *a* are biogeochemically significant. For example, the asymptotic errors for pCO_2 and $\Delta O_2/Ar$ are on order 10% of measured signals. Since CO_2 fluxes scale linearly with pCO_2, this would translate directly into an equivalent error in air-sea flux calculations.

There are several physical processes that likely contribute to the short-length-scale variability in the Ross Sea. Weak stratification in polar regions permits significant vertical transport of subsurface water masses which have chemical properties distinct from those of surface waters. This vertical entrainment is further enhanced by horizontal advection of buoyancy and lateral stirring, which have been shown to drive much of the sub-mesoscale variability in surface water pCO_2 (Mahadevan et al., 2004). This mechanism is also relevant for all of the gases we measured in the Ross Sea. The model of Mahadevan et al. (2004) used a horizontal resolution of $2\,km \times 2\,km$. Our data suggest that significant variability may extend to even smaller scales than this, associated with (for example) ice-melt processes. Resolving variability at these scales will be an important step towards fully understanding the mechanistic controls on biogeochemical cycles in the Ross Sea and other Antarctic polynya waters.

5. Conclusions

Using a novel analytical approach, we have characterized previously undocumented fine-scale variability in pCO_2, $\Delta O_2/Ar$ and DMS in the Ross Sea polynya that is coupled to heterogeneity in the underlying physical and biological fields (*e.g.* sea ice cover and Chl *a*). The length scales of this variability are not easily captured using hydrographic surveys at discrete sampling stations. While fine-scale variability was apparent during both of our surveys, broad-scale gas distributions exhibited significant differences between the early spring and summer. During the early spring time, the net heterotrophic signal of recently ice-free waters drives a strong air-sea exchange gradient which pushes surface waters towards atmospheric equilibrium. This air-sea flux exerts a particularly large effect on O_2 relative to CO_2, resulting in high apparent rates of O_2 increase per unit CO_2 drawdown and a C–O stoichiometry which differs significantly from a purely biological signal. As the early spring bloom develops, enhanced stratification (due to surface warming and decreased wind speeds) increases the efficiency of air-sea exchange and stimulates NCP in the shoaling mixed layer. These two effects drive the system towards a steady state, where net O_2 production (and CO_2 consumption) is balanced by sea-air fluxes. As these conditions persist into the later summer period, changes in surface gas concentrations per unit NCP decrease, and additional spatial variance is introduced from small-scale mixing processes.

Surface water DMS concentrations also show large seasonal differences, with significantly higher concentrations observed during the early growth season. The elevated spring-time DMS concentrations may partly reflect the enhanced biomass of *Phaeocystis* during this time. It is also likely, however, that reduced DMS turnover rates are partially responsible for the accumulation of high concentrations in the early season polynya. Conversely, rapid biological consumption of DMS may act to decouple DMS concentrations with biological productivity signals (*e.g.* O_2/Ar, pCO_2, Chl *a*). Future studies coupling underway MIMS measurements with focused process studies will provide significantly new insight onto the importance of different environmental and ecological factors controlling DMS emissions from the Ross Sea, and a more comprehensive understanding of this region's impact on global climate regulation.

Acknowledgments

This work was supported by the US National Science Foundation, Office of Polar Programs (NSF-OPP-0338097), and funding from the Natural Sciences and Engineering Research Council of Canada (PDT). We thank the Captain and crew of the R.V./IB *Nathanial B. Palmer* for logistical assistance, as well as the entire CORSACS science team for support at sea and valuable intellectual input. We also thank Laurie Juranak (NOAA, PMEL) for the IRMS analysis of O_2/Ar calibration samples.

References

Arrigo, K.R., DiTullio, G.R., Dunbar, R.B., Robinson, D.H., VanWoert, M., Worthen, D.L., Lizotte, M.P., 2000. Phytoplankton taxonomic variability in nutrient utilization and primary production in the Ross Sea. Journal of Geophysical Research—Oceans 105 (C4), 8827–8845.

Arrigo, K.R., Dunbar, R., Lizotte, M.P., Robinson, D.H., 2002. Taxon-specific differences in C/P and N/P drawdown for phytoplankton in the Ross Sea, Antarctica. Geophysical Research Letters 29 (19), 1938.

Arrigo, K.R., Robinson, D.H., Worthen, D.L., Dunbar, R.B., DiTullio, G.R., VanWoert, M., Lizotte, M.P., 1999. Phytoplankton community structure and the drawdown of nutrients and CO_2 in the Southern Ocean. Science 283 (5400), 365–367.

Arrigo, K.R., van Dijken, G., Long, M.C., 2008. Coastal Southern Ocean: a strong anthropogenic CO_2 sink. Geophysical Research Letters, 35.

Arrigo, K.R., Weiss, A.M., Smith Jr., W.O., 1998a. Physical forcing of phytoplankton dynamics in the southwestern Ross Sea. Journal of Geophysical Research 103 (c1), 1007 1097JC02326.

Arrigo, K.R., Worthen, D.L., Schnell, A., Lizotte, M.P., 1998b. Primary production in Southern Ocean waters. Journal of Geophysical Research 103 (C8), 15,587–515,600.

Ayers, G.P., Cainey, J.M., 2007. The CLAW hypothesis: a review of the major developments. Environmental Chemistry 4 (6), 366–374.

Belviso, S., Kim, S.K., Rassoulzadegan, F., Krajka, B., Nguyen, B.C., Mihalopoulos, N., Buatmenard, P., 1990. Production of dimethylsulfonium propiopnate (DMSP) and dimethylsulfide (DMS) by a microbial foodweb. Limnology and Oceanography 35 (8), 1810–1821.

Boccaletti, G., Ferrari, R., Fox-Kemper, B., 2007. Mixed layer instabilities and restratification. Journal of Physical Oceanography 37 (9), 2228–2250.

Boucher, O., Moulin, C., Belviso, S., Aumont, O., Bopp, L., Cosme, E., von Kuhlmann, R., Lawrence, M.G., Pham, M., Reddy, M.S., Sciare, J., Venkataraman, C., 2003. DMS atmospheric concentrations and sulphate aerosol indirect radiative forcing: a sensitivity study to the DMS source representation and oxidation. Atmospheric Chemistry and Physics 3, 49–65.

Cavalieri, D., Gloerson, P., Zwally, J., 1990 (Updated 2006). Maslanik, J., Stroeve, J. (Eds.), DMSP SSM/I daily polar gridded sea ice concentrations. National Snow and Ice Data Center, Digital Media, Boulder, CO.

Coale, K.H., Wang, X., Tanner, S.J., Johnson, K.S., 2003. Phytoplankton growth and biological response to iron and zinc addition in the Ross Sea and Antarctic Circumpolar Current along 170 W. Deep-Sea Research II—Topical Studies in Oceanography 50 (3–4), 635–653.

Craig, H., Hayward, T., 1987. Oxygen supersaturation in the ocean—biological versus physical contributions. Science 235 (4785), 199–202.

Dacey, J.W.H., Wakeham, S.G., 1986. Oceanic dimethylsulfide production during zooplankton grazing on phytoplankton. Science 233 (4770), 1314–1316.

del Valle, D.A., Kieber, D.J., Toole, D.A., Brinkley, J., Kiene, R.P., 2009. Biological consumption of dimethylsulfide (DMS) and its importance in DMS dynamics in the Ross Sea, Antarctica. Limnology and Oceanography 54 (3), 785–798.

Derevianko, G.J., Deutsch, C., Hall, A., 2009. On the relationship between ocean DMS and solar radiation. Geophysical Research Letters 36, L17606.

Ditullio, G.R., Smith, W.O., 1995. Relationship between dimethylsulfide and phytoplankton pigment concentrations in the Ross Sea, Antarctica. Deep-Sea Research I—Oceanographic Research Papers 42 (6), 873–892.

DiTullio, G.R., Smith, W.O., 1996. Spatial patterns in phytoplankton biomass and pigment distributions in the Ross Sea. Journal of Geophysical Research—Oceans 101 (C8), 18467–18477.
DiTullio, G.R., Grebmeier, J.M., Arrigo, K.R., Lizotte, M.P., Robinson, D.H., Leventer, A., Barry, J.B., VanWoert, M.L., Dunbar, R.B., 2000. Rapid and early export of *Phaeocystis antarctica* blooms in the Ross Sea, Antarctica. Nature 404 (6778), 595–598.
DiTullio, G.R., Geesey, M.E., 2002. Photosynthetic pigments in marine algae and bacteria. In: Bitton, G. (Ed.), Encyclopedia of Environmental Microbiology, vol. 5. J. Wiley and Sons, New York, NY, pp. 2453–2470.
DiTullio, G.R., Dunbar, R.B., 2003. Biogeochemistry of the Ross Sea—an introduction. In: DiTullio, G.R., Dunbar, R.B. (Eds.), Biogeochemistry of the Ross Sea, vol. 78. AGU Antarctic Research Series, Washington, DC, pp. 1–4.
Doney, S.C., Glover, D.M., McCue, S.J., Fuentes, M., 2003. Mesoscale variability of Sea-viewing Wide Field-of-view Sensor (SeaWiFS) satellite ocean color: global patterns and spatial scales. Journal of Geophysical Research—Oceans 108 (C2), 15.
Emerson, S., Stump, C., Wilbur, D., Quay, P., 1999. Accurate measurement of O_2, N_2, and Ar gases in water and the solubility of N_2. Marine Chemistry 64 (4), 337–347.
Feng, Y., Hare, C.E., Rose, J.M., Handy, S.M., DiTullio, G.R., Lee, P.A., Smith, W.O., Peloquin, J., Tozzi, S., Sun, J., Zhang, Y., Dunbar, R.B., Long, M.C., Sohst, B., Lohan, M., Hutchins, D.A., 2010. Interactive effects of iron, irradiance and CO_2 on Ross Sea phytoplankton. Deep-Sea Research I 57 (3), 368–383.
Fox-Kemper, B., Ferrari, R., Hallberg, R., 2008. Parameterization of mixed layer eddies. Part I: Theory and diagnosis. Journal of Physical Oceanography 38 (6), 1145–1165.
Garcia, H.E., Gordon, L.I., 1992. Oxygen solubility in seawater: better fitting equations. Limnology and Oceanography 37, 1307–1312.
Gondwe, M., Krol, M., Gieskes, W., Klaassen, W., de Baar, H., 2003. The contribution of ocean-leaving DMS to the global atmospheric burdens of DMS, MSA, SO_2, and NSS SO_4^{-2}. Global Biogeochemical Cycles 17, 2.
Gordon, L.I., Codispoti, L.A., Jennings, J.C., Millero, F.J., Morrison, J.M., Sweeney, C., 2000. Seasonal evolution of hydrographic properties in the Ross Sea, Antarctica, 1996–1997. Deep-Sea Research II 47 (15–16), 3095–3117.
Gruber, N., Keeling, C.D., Stocker, T.F., 1998. Carbon-13 constraints on the seasonal inorganic carbon budget at the BATS site in the northwestern Sargasso Sea. Deep-Sea Research I 45 (4–5), 673–717.
Gueguen, C., Tortell, P.D., 2008. High-resolution measurement of Southern Ocean CO_2 and O_2/Ar by membrane inlet mass spectrometry. Marine Chemistry 108 (3–4), 184–194.
Hales, B., Takahashi, T., 2004. High-resolution biogeochemical investigation of the Ross Sea, Antarctica, during the AESOPS (U.S. JGOFS) Program. Global Biogeochemical Cycles 18 (3), 24.
Jacobs, S.S., 2004. Bottom water production and its links with the thermohaline circulation. Antarctic Science 16 (4), 427–437.
Kaiser, J., Reuer, M.K., Barnett, B., Bender, M.L., 2005. Marine productivity estimates from continuous O_2/Ar ratio measurements by membrane inlet mass spectrometry. Geophysical Research Letters 32, 19.
Kettle, A.J., Andreae, M.O., Amouroux, D., Andreae, T.W., Bates, T.S., Berresheim, H., Bingemer, H., Boniforti, R., Curran, M.A.J., DiTullio, G.R., Helas, G., Jones, G.B., Keller, M.D., Kiene, R.P., Leck, C., Levasseur, M., Malin, G., Maspero, M., Matrai, P., McTaggart, A.R., Mihalopoulos, N., Nguyen, B.C., Novo, A., Putaud, J.P., Rapsomanikis, S., Roberts, G., Schebeske, G., Sharma, S., Simo, R., Staubes, R., Turner, S., Uher, G., 1999. A global database of sea surface dimethylsulfide (DMS) measurements and a procedure to predict sea surface DMS as a function of latitude, longitude, and month. Global Biogeochemical Cycles 13 (2), 399–444.
Kiene, R.P., Kieber, D.J., Slezak, D., Toole, D.A., del Valle, D.A., Bisgrove, J., Brinkley, J., Rellinger, A., 2007. Distribution and cycling of dimethylsulfide, dimethylsulfoniopropionate, and dimethylsulfoxide during spring and early summer in the Southern Ocean south of New Zealand. Aquatic Sciences 69 (3), 305–319.
Kiene, R.P., Linn, L.J., 2000. The fate of dissolved dimethylsulfoniopropionate (DMSP) in seawater. Tracer studies using S^{35}-DMSP. Geochimica et Cosmochimica Acta 64 (16), 2797–2810.
Kiene, R.P., Slezak, D., 2006. Low dissolved DMSP concentrations in seawater revealed by small-volume gravity filtration and dialysis sampling. Limnology and Oceanography Methods 4, 80–95.
Long, M.C., 2010. Upper Ocean physical and ecological dynamics in the Ross Sea, Antarctica. Ph.D. Thesis, Stanford University.
Long, M.C., Thomas, L.N., Dunbar, R.B. Physical dynamics controlling seasonal evolution and timescales of variability in mixing depths in the Ross Sea, Anarctica. Global Biogeochemical Cycles, submitted for publication-a.
Long, M.C., Dunbar, R.B., Tortell, P.D., Smith, W.O., Mucciarone, D.A. Vertical structure, seasonal drawdown, and net community production in the Ross Sea. Journal of Geophysical Research, submitted for publication-b.
Mackey, M.D., Mackey, D.J., Higgins, H.W., Wright, S.W., 1996. CHEMTAX—a program for estimating class abundances from chemical markers: application to HPLC measurements of phytoplankton. Marine Ecology—Progress Series 144, 265–283.
Mahadevan, A., Levy, M., Memery, L., 2004. Mesoscale variability of sea surface pCO_2: what does it respond to? Global Biogeochemical Cycles 18, 1.
Malin, G., Wilson, W.H., Bratbak, G., Liss, P.S., Mann, N.H., 1998. Elevated production of dimethylsulfide resulting from viral infection of cultures of *Phaeocystis pouchetii*. Limnology and Oceanography 43 (6), 1389–1393.
Merzouk, A., Levasseur, M., Scarratt, M.G., Michaud, S., Rivkin, R.B., Hale, M.S., Kiene, R.P., Price, N.M., Li, W.K.W., 2006. DMSP and DMS dynamics during a mesoscale iron fertilization experiment in the Northeast Pacific—Part II: Biological cycling. Deep-Sea Research I 53 (20–22), 2370–2383.
Muller, P., Li, X.P., Niyogi, K.K., 2001. Non-photochemical quenching. A response to excess light energy. Plant Physiology 125 (4), 1558–1566.
Nemcek, N., Ianson, D., Tortell, P.D., 2008. A high-resolution survey of DMS, CO_2, and O_2/Ar distributions in productive coastal waters. Global Biogeochemical Cycles 22, 2.
Reuer, M.K., Barnett, B.A., Bender, M.L., Falkowski, P.G., Hendricks, M.B., 2007. New estimates of Southern Ocean biological production rates from O_2/Ar ratios and the triple isotope composition of O_2. Deep-Sea Research I—Oceanographic Research Papers 54 (6), 951–974.
Rose, J.M., Feng, Y., DiTullio, G.R., Dunbar, R.B., Hare, C.E., Lee, P.A., Lohan, M., Long, M., Smith, W.O., Sohst, B., Tozzi, S., Zhang, Y., Hutchins, D.A., 2009. Synergistic effects of iron and temperature on Antarctic phytoplankton and microzooplankton assemblages. Biogeosciences 6 (12), 3131–3147.
Saltzman, E.S., King, D.B., Holmen, K., Leck, C., 1993. Experimental determination of the diffusion coefficient of dimethylsulfide in water. Journal of Geophysical Research 98 (C9).
Sandrini, S., Ait-Ameur, N., Rivaro, P., Massolo, S., Touratier, F., Tositti, L., Goyet, C., 2007. Anthropogenic carbon distribution in the Ross Sea, Antarctica. Antarctic Science 19 (3), 395–407.
Sedwick, P.N., DiTullio, G.R., 1997. Regulation of algal blooms in Antarctic shelf waters by the release of iron from melting sea ice. Geophysical Research Letters 24 (20), 2515–2518.
Sedwick, P.N., DiTullio, G.R., Mackey, D.J., 2000. Iron and manganese in the Ross Sea, Antarctica: seasonal iron limitation in Antarctic shelf waters. Journal of Geophysical Research 105 (C5), 11,321–311,336.
Sedwick, P.N., Marsay, C.M., Aguilar-Islas, A.M., Lohan, M.C., Sohst, B.M., Long, M.C., Arrigo, K.R., Bruland, K.W., DiTullio, G.R., Dunbar, R.B., Saito, M.A., Smith, W.O. Early-season iron depletion in the Ross Sea polynya: Implications for iron dynamics on the Antarctic continental shelf. Journal of Geophysical Research—Oceans, submitted for publication.
Simó, R., Pedrós-Alió, C., Malin, G., Grimalt, J.O., 2000. Biological turnover of DMS, DMSP and DMSO in contrasting open-sea waters. Marine Ecology—Progress Series 203, 1–11.
Simo, R., Dachs, J., 2002. Global ocean emission of dimethylsulfide predicted from biogeophysical data. Global Biogeochemical Cycles 16, 4.
Simó, R., 2004. From cells to globe: approaching the dynamics of DMS (P) in the ocean at multiple scales. Canadian Journal of Fisheries and Aquatic Sciences 61 (5), 673–684.
Smith, W.O., Anderson, R.F., 2003. US Southern Ocean JGOFS Program (AESOPS)—Part III. Deep-Sea Research I 50 (3–4), 529–531.
Smith, W.O., Anderson, R.F., Moore, J.K., Codispoti, L.A., Morrison, J.M., 2000. The US Southern Ocean Joint Global Ocean Flux Study: an introduction to AESOPS. Deep-Sea Research I 47 (15–16), 3073–3093.
Smith, W.O., Gordon, L.I., 1997. Hyperproductivity of the Ross Sea (Antarctica) polynya during austral spring. Geophysical Research Letters 24 (3), 233–236.
Stefels, J., Dijkhuizen, L., 1996. Characteristics of DMSP-lyase in *Phaeocystis* sp. (Prymnesiophyceae). Marine Ecology—Progress Series 131 (1–3), 307–313.
Stefels, J., Steinke, M., Turner, S., Malin, G., Belviso, S., 2007. Environmental constraints on the production and removal of the climatically active gas dimethylsulphide (DMS) and implications for ecosystem modelling. Biogeochemistry 83 (1–3), 245–275.
Stefels, J., Vanboekel, W.H.M., 1993. Production of DMS from dissolved DMSP in axenic cultures of the marine phytoplankton species *Phaeocystis* sp. Marine Ecology—Progress Series 97 (1), 11–18.
Sunda, W., Kieber, D.J., Kiene, R.P., Huntsman, S., 2002. An antioxidant function for DMSP and DMS in marine algae. Nature 418 (6895), 317–320.
Sweeney, C., Hansell, D.A., Carlson, C.A., Codispoti, L.A., Gordon, L.I., Marra, J., Millero, F.J., Smith, W.O., Takahashi, T., 2000. Biogeochemical regimes, net community production and carbon export in the Ross Sea, Antarctica. Deep-Sea Research II 47 (15–16), 3369–3394.
Takahashi, T., Sutherland, S.C., Wanninkhof, R., Sweeney, C., Feely, R.A., Chipman, D.W., Hales, B., Friederich, G., Chavez, F., Sabine, C., Watson, A., Bakker, D.C.E., Schuster, U., Metzl, N., Yoshikawa-Inoue, H., Ishii, M., Midorikawa, T., Nojiri, Y., Kortzinger, A., Steinhoff, T., Hoppema, M., Olafsson, J., Arnarson, T.S., Tilbrook, B., Johannessen, T., Olsen, A., Bellerby, R., Wong, C.S., Delille, B., Bates, N.R., de Baar, H.J.W., 2009. Climatological mean and decadal change in surface ocean pCO_2, and net sea-air CO_2 flux over the global oceans. Deep-Sea Research II—Topical Studies in Oceanography 56 (8–10), 554–577.
Thomas, L., Ferrari, R., 2008. Friction, frontogenesis, and the stratification of the surface mixed layer. Journal of Physical Oceanography 38 (11), 2501–2518.
Toole, D.A., Kieber, D.J., Kiene, R.P., White, E.M., Bisgrove, J., del Valle, D.A., Slezak, D., 2004. High dimethylsulfide photolysis rates in nitrate-rich Antarctic waters. Geophysical Research Letters 31, 11.
Tortell, P.D., 2005. Dissolved gas measurements in oceanic waters made by membrane inlet mass spectrometry. Limnology and Oceanography: Methods 3, 24–37.
Tortell, P.D., Long, M.C., 2009. Spatial and temporal variability of biogenic gases during the Southern Ocean spring bloom. Geophysical Research Letters, 36.
Trumbore, S.E., Jacobs, S.S., Smethie, W.M., 1991. Chlorofluorocarbon evidence for rapid ventilation of the Ross Sea. Deep-Sea Research Part A—Oceanographic Research Papers 38 (7), 845–870.
Vallina, S.M., Simo, R., Gasso, S., De Boyer-Montegut, C., del Rio, E., Jurado, E., Dachs, J., 2007. Analysis of a potential "solar radiation dose-dimethylsulfide-cloud

condensation nuclei" link from globally mapped seasonal correlations. Global Biogeochemical Cycles 21, 2.
Vlahos, P., Monahan, E.C., 2009. A generalized model for the air-sea transfer of dimethyl sulfide at high wind speeds. Geophysical Research Letters, 36.
Wanninkhof, R., 1992. Relationship between wind speed and gas exchange over the Ocean. Journal of Geophysical Research 97 (C5), 7373–7382.
Weiss, R.F., 1974. Carbon dioxide in seawater: the solubility of an ideal gas. Marine Chemistry 2, 203–215.
Zubkov, M.V., et al., 2002. Rapid turnover of dissolved DMS and DMSP by defined bacterioplankton communities in the stratified euphotic zone of the North Sea. Deep-Sea Research II—Topical Studies in Oceanography 49 (15), 3017–3038.